MASTER'S THESIS

FABRICATION AND ANALYSIS OF GLUCOSE SENSOR

Faculty of Electrical Engineering, Mathematics and Computer Science (EEMCS)

Dileep Rangaswamaiah Chennaveeranahalli

Department of Integrated Devices and Systems
University of Twente

EXAMINATION COMMITTEE

DR.IR. R.J. Wiegerink

DR.IR. W. Olthuis

Prof.DR.IR. JC LÖtters

UNIVERSITY OF TWENTE.

ABSTRACT

Millions of people worldwide suffer from Diabetes mellitus caused due to inadequate production of insulin hormones leading to varying glucose concentrations in the blood and causing a series of problems. Hence, Individuals suffering from such a disease need close monitoring and management of glucose levels in their blood. The traditional way of monitoring is by finger pricking and measuring blood glucose in an external monitoring device and then taking an appropriate dose of insulin shots or glucose-rich edibles in the latter case. It is a cyclic process every day, exposing patients to inflammation and might cause discomfort. Hence, current research is more toward self-monitoring using real-time Continuous Glucose Monitoring (CGM) devices. This project aims at designing a sensor for one such device.

Before integrating the sensor into the continuous monitoring device, it is essential to know the behavior of the sensor. We chose an amperometric enzymatic sensor design, assuming it could be implanted into the dermal region of the skin to measure glucose concentration in the IF (Interstitial Fluid) between the body cells. The fabrication process flow for the third-generation amperometric sensor with Au nanoparticles was made to achieve a high response sensitivity. However, since more than 70% of this design coincides with the first-generation devices (with H_2O_2 detection) and the expensive material requirements and complexity, we decided to fabricate the first-generation devices and analyze their behavior. We designed different geometry with varied dimensions to examine its working with the three-electrode amperometric approach. Part of the fabrication was done at the MESA+ institute and was later post-processed in the external laboratory to achieve the expected sensor. As a part of the post-processing, we used PBS buffer solution with the cyclic voltammetric approach to form a Pseudo-reference metal electrode by oxidizing Ir metal on-chip using the AIROF technique. The fabricated sensors did not behave as expected due to the failure to attain pseudo reference as a part of its design. Due to the lack of activation cycles in developing IrO_x on top of Ir microelectrodes to act as a pseudo reference, our final glucose measurements did not provide desired results.

ACKNOWLEDGEMENT

I want to thank my supervisor dr.Ir. R.J. Wiegerink for providing me with this opportunity, motivating and for his unconditional support throughout this project. I extend my gratitude to the daily supervisor Sabrine Mejri, Ph.D., for supporting me in this project. My sincere appreciation for dr.Ir. W. Olthuis for his insight on this work. I want to thank K.M Batenburg and M.J. de Boer for fabricating my design on the Silicon wafer at the MESA+ institute. Further, I extend my appreciation to Ing. RGP Sanders for his assistance in the laboratory. I thank M.A. Smithers for providing me with HRSEM images of the samples at the MESA+ institute. Further, I thank dr. Y Bu for helping me with the XPS analysis at the MESA+ institute. I want to thank my friends and family for their encouragement throughout this work. Finally, I would like to thank my parents for their unconditional support throughout this project, especially during the COVID-19 pandemic.

I want to dedicate this work to the demised family members and the lost souls worldwide during the COVID-19 pandemic.

TABLE OF CONTENTS

LIST OF FIGURES

LIST OF TABLES

LIST OF ABBREVIATIONS

T1DM	Type 1 Diabetes Mellitus
T2DM	Type 2 Diabetes Mellitus
CGM	Continuous Glucose Monitoring
AP	Artificial Pancreas
CSII	Continuous Subcutaneous Insulin Infusion
IF	Interstitial Fluid
WE	Working Electrode
CE	Counter Electrode (Auxiliary Electrode)
RE	Reference Electrode
AA	L-Ascorbic Acid
UA	Uric Acid
PU	Polyurethane
NP	Nanoparticle
Q-RE	Quasi-Reference Electrode
CSC	Charge Storage Capacity
EIROF	Electrodeposited IrO_x film
TIROF	Thermal IrO_x film
SIROF	Sputtering IrO_x film
AIROF	Activated IrO_x film
CV	Cyclic Voltammetry
OCP	Open Circuit Potential

CHAPTER 1. INTRODUCTION

Food intake (primarily carbohydrates) in the human body is converted to Glucose (the primary energy source at the cellular level) by the digestive tract and released into the blood. This blood Glucose concentration triggers the beta cells of the pancreas to produce a hormone called Insulin, which is released to the blood as shown in Figure 1. Blood transports Glucose and Insulin to various body cells. However, in the body cell, Insulin in the blood regulates the absorption of Glucose. Inadequate Insulin concentration in the blood causes varied Glucose concentrations in the blood leading to toxicity and a series of other problems. This condition is called Diabetes Mellitus. Diabetes Mellitus is classified into Type 1 (T1DM) and Type 2 (T2DM), where the former is an autoimmune disease that often shows up at the early stages of the human lifespan obtained through ancestors in which the immune system destroys the beta cells of the pancreas leading to inadequate production of Insulin. The latter is majorly diet oriented caused due to over-nutrition, which builds up over time in the human lifespan leading to excess glucose concentration compared to the produced Insulin[1].

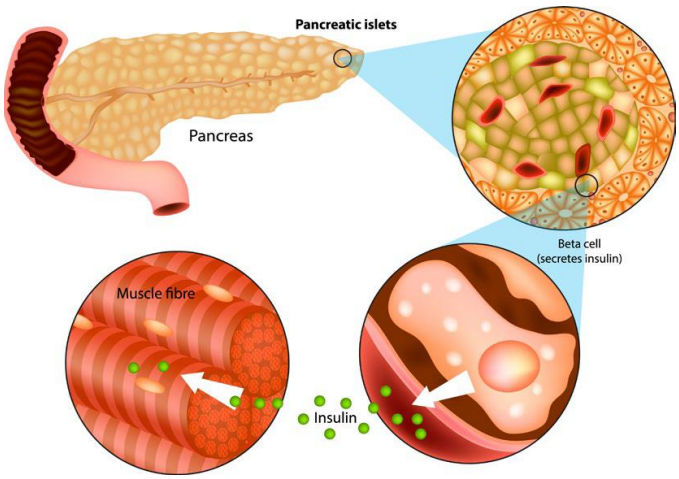

Figure 1: Pictorial representation of the production and transport of Insulin in the human body[1]

In 2021, approximately 537 million people aged 20-79 years were suffering from diabetes [2], projected to increase by 25% in 2030 and, by 2045, 51% [3]. The Netherlands has 100-125 thousand patients, rising by 3.8% annually [2-3].

The unstable glucose level caused by the disease can lead to tremendous complications, the least of which is hypoglycemia (low blood sugar), which is below 70-55mg/dL of plasma glucose concentration [5] and hyperglycemia (high blood sugar), which is above 125-180mg/dL of plasma glucose concentration [6]. Thus, appropriate management is essential. Type 1 and Type 2 patients must self-manage their blood glucose levels during the day. The traditional way to do so used to be by finger pricking. However accurate, this method can expose the patients to different risks, such as infections, and can present a source of discomfort.

Hence, real-time continuous glucose monitoring (CGM) is conducted to improve self-monitoring and avoid inflammations. Researchers and industries are competing in the field of CGM with unified goals in mind, which are mainly pain-free monitoring and precise glycemic evolution for better control of preprandial (before a meal) and postprandial (after a meal) [7].

Different products englobing different techniques and materials are available to ensure the optimum glycemic management [8]–[10], whether it is an enzymatic sensor [11]–[15] or enzyme-free [16]–[19], invasive or non-invasive, or even implantable.

However, the CGM does not only include the glucose sensor. It is a closed-loop system where the algorithm evaluates the signal from the sensor in the artificial pancreas (AP), which sends the appropriate amount of Insulin using the infusion device.

In this project, the basis for our system is as described above, bringing together Inreda Diabetic's advanced AP, U-Needle's intradermal delivery technology, and the University of Twente’s sensor expertise to collaborate in Microneedle Artificial Pancreas (MAP), which aims to deliver Insulin and Glucagon faster than the widely used continuous subcutaneous insulin infusion (CSII) systems. Thus, reducing postprandial spikes and achieving an improved time-in-range. To do this,

a trivial subcutaneous infusion system, which provides relatively slow uptake, is to be replaced with a high-response intradermal infusion system, which creates a new system for continuous intradermal Insulin and glucagon infusion. It is assumed that this would end manual glucose management, even during meal intake [20]. In AP systems, intradermal infusion of Glucagon and Insulin are used, making them cutting-edge devices in the field. The Microneedle integrated sensor and AP are expected to increase the life quality of millions suffering from diabetes significantly.

This project aims to design and test the glucose sensor, which could be integrated into the existing intradermal infusion needle, as shown in Figure 2. However, before it can be integrated into the needle, the first step is to replicate the current sensor design from [21], [22], fabricate the design, and investigate the behavior by comparing the results.

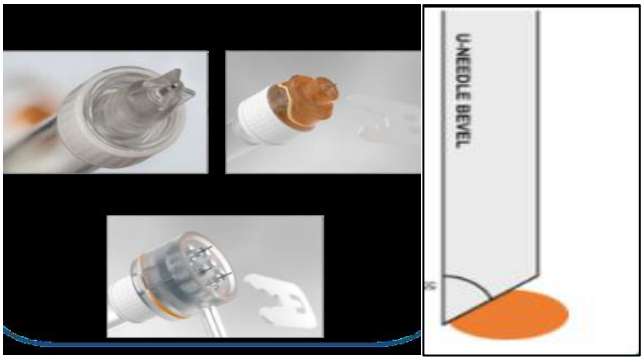

Figure 2: Design of the intradermal microneedle fabricated by UNeedle

1.1. REQUIREMENTS OVERVIEW

The device fabricated and tested in this work should meet the following requirements when tested in both in-vitro and in-vivo environments. However, this work is narrowed to in-vitro measurements, and the in-vivo measures are mentioned for future reference. Table 1 represents the in-vitro measurement parameters of the design in [21], [22] at room temperature.

Electrode dimension (μm^2)	Integrated to needle (lumen diameter in µm)	Additional coating (µm)	Impurities present, if any (UA, AA in µM)	Sensitivity in linear range (nA/mM)	Average response time (s)	Maximum sensing variation rate ($mgdL^{-1} min^{-1}$)	Maximum Physiological variation rate ($mgdL^{-1} min^{-1}$)	Ref.
700x70	Yes (90)	No	NO	2.44	315	9.5	3	[21]
170x70	No	Yes (Polyurethane, 19.5 ±4.5)	Yes (100 each)	1.51	300	10	3	[22]

Table 1: Represents the key parameters and outcome of the sensor mentioned in [21], [22] *at room temperature and in-vitro conditions*

1.1.1. IN-VITRO ENVIRONMENT

From [21], when the sensor with electrode dimensions 700x70 μm^2 is integrated into a hollow cavity or lumen of a needle. Tested in a buffer solution without additional impurities shows the sensitivity of a 2.44 nA rise in current output per mM glucose concentration in the linear range and an average response time of 315 s. The maximum sensing variation rate of 9.5mg/dL/min was obtained, which was way more than the maximum physiological glucose variation rate, 3 mg/dL/min [23] as shown in Table 1.

From [22], the sensor set with electrode dimensions 170x70 μm^2 and an additional perm-selective layer, polyurethane of thickness 19.5 ±4.5 µm, deposited (to obtain linearity) without being integrated into the microneedle. It showed a sensitivity of 1.51nA/mM in the linear range in the buffer solution with impurities like electroactive species like L-ascorbic acid (AA) and uric acid (UA) of each 100 µM. An average response time of 300 s. Maximum sensing variation of

10mg/dL/min was observed compared to 3 mg/dL/min physiological variation rate as shown in Table 1.

1.1.2. IN-VIVO ENVIRONMENT

From [21], following in-vitro measurements discussed in the previous section, when integrated into a lumen of the needle was tested in an in-vivo environment, had a response time of 10 min in interstitial fluid (IF) in the dermis layer of the skin.

Commercially available advanced CGM systems like Abbott's Freestyle Libre devices [24] respond every few minutes to the monitoring device, last for 14 days without losing accuracy in low glucose concentrations, and go deep into the hypodermis layer of the skin. That is from [25], 93.2% and 92.1% of sensor accuracy within ±20%/20 mg/dL of YSI reference [26] with a time delay of 2.4 ± 4.6 and 2.1 ± 5.0 minutes when tested in-vivo for adults (18 years+) and pediatric (4-17 years) respectively.

1.2. THESIS OUTLINE

As discussed above, this project aims to replicate the existing sensor design from [21], [22] and analyze the results before an advanced design with a high response could be integrated into the Intradermal infusion needle as the fabrication of the later include more than 70% of the process flow of the former.

In this work, a possible design choice using a literature study is first discussed in Chapter 2. It provides essential information on the analyte (Glucose) of interest and critical parameters in sensing biochemicals. Then the existing transduction techniques have been described, ending with our case's best method of choice. Further, the chosen technique and its working are elaborated. Furthermore, it is categorized based on the history of research.

Chapter 3 discusses the design of the test samples and fabrication process technologies to achieve the senor configurations from [21], [22] in the cleanroom. Later, process technology for future design with advanced Au nanoparticle (NP) is elaborated.

Chapter 4 describes the post-processing outside the cleanroom facility. At first, the experimental method to oxidize Ir to form a Reference electrode (RE) on-chip and the materials used. Later, it discusses the practical approach of functionalizing the senor with the enzyme.

Chapter 5 mentions the experimental setup to measure the Glucose concentration and materials required for it. Also, the results from [21], [22] are discussed to compare the results.

Further, measurements and analysis of glucose concentration readouts and IrOx RE formation are discussed in Chapter 6.

Chapter 7 describes the conclusion and future recommendations concerning it.

CHAPTER 2. LITERATURE STUDY

Glucose ($C_6H_{12}O_6$) is one of the building blocks of sugar and belongs to the group of carbohydrates. It belongs to the sub-category monosaccharide, categorized based on size and complexity. It is the most abundant monosaccharide amongst the three most seen monosaccharides (Glucose, Fructose, and Galactose). All three monosaccharides mentioned above possess the same chemical formula but different structures (Isomers). However, they can be converted from one form to another. The only sugar living creatures can use for energy at the cellular level is Glucose. Figure 3(a) shows the structure of Glucose. Glucose possesses a molecular mass of 180.156 g/mol, a size of 1nm, and is charge neutral. From Figure 3 (b), Glucose is much smaller than cancer cells, bacteria, viruses, or antibodies. Hence a novel approach is required for sensing applications.

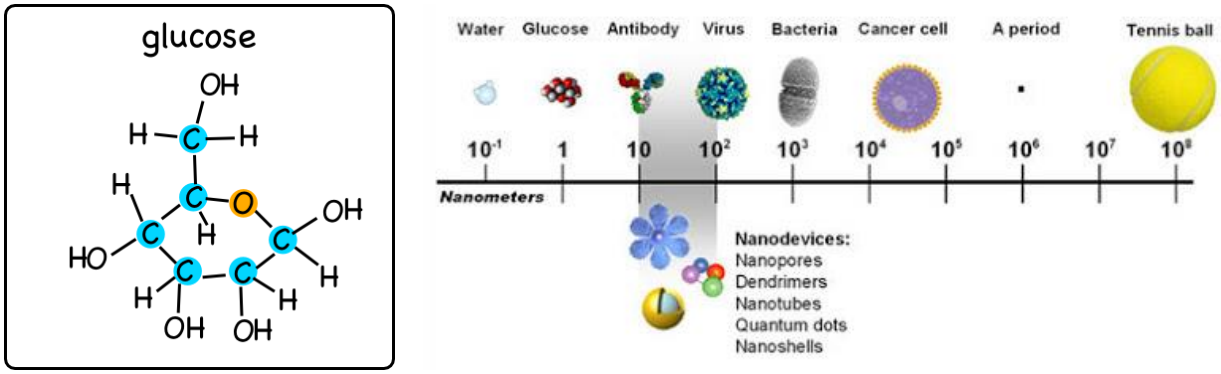

a) b)

Figure 3: a) Molecular structure of Glucose, b) Pictorial representation showing the size of a different biomolecule with respect to a tennis ball [27].

A wide variety of transduction methods could be utilized in chemical sensors, and the recognition process could hardly be descriptively generalized. However, for a better understanding of the process, Eq.(1) represents a generalized chemical reaction (only to explain in our case), where A is the analyte, R is the recognition receptor, and P is the product obtained due to the interaction between analyte and receptor. Also, subscript S represents a sample, SE represents the sensing

$$A_{(s)} + R_{(SE)} \rightleftharpoons P \qquad (1)$$

element, and the double arrow indicates that the recognition process is a reversible reaction at equilibrium.

From [27], critical parameters for the transduction of chemicals or biomolecules in the sensing application includes :

- Mass
- Charge
- Electron affinity
- Optical index

That is, when an analyte A interacts with the recognition species R, it forms product P (from Eq. (1)). Making this interaction more specific to the analyte used, one could measure the mass of the product obtained after the interaction, which determines the concentration of the analyte in the given medium. It is mass-dependent.

Alternatively, when A interacts with R can lead to changes in the electrical property of the material/medium, proportional to the analyte concentration in the medium. It is purely charge-dependent.

Alternatively, when A interacts with R, it could produce ionic species as a byproduct and deal with the electron transfer reactions due to the ability of the analyte or its byproduct to donate or accept electrons. It is purely dependent on electron affinity.

Alternatively, when analyte A interacts with R, it could be recognized by employing the electromagnetic radiative property of the product and byproduct specific to the analyte used. It is based on an optical index [28].

In general, different approaches are used in sensing chemicals and biomolecules and are not limited to [28], [27]:

- **Thermometric transduction:** based on thermal effects of the recognition process, which leads to a change in temperature.
- **Transduction based on mechanical effect:** based on the change in the overall mass of the sensing element.
- **Resistive and capacitive transduction:** based on the change in the material's electrical property causing electrical resistivity to change as a function of the analyte concentration (Resistive transduction), change in dielectric constant leading to capacitive change due to the analyte in the structure (Capacitive transduction).
- **Electrochemical transduction:** is based on ion transport, ion distribution, and electron-transfer reaction at the solution interface with a solid conductor or electrode.
- **Optical transduction:** based on the interaction of electromagnetic radiation with matter analyzed using spectrochemical methods.

However, in our case, the transduction based on mechanical effect is not possible because the glucose molecule is too small to be detected by the regular mass-based sensor (Eg: Cantilever mass sensor). Even though specific shapes could be achieved on top of the cantilever beam, the recognition process becomes complex due to interferents in the IF (Interstitial Fluid). Since Glucose is charge neutral species, resistive and capacitive transductions are not possible. Also, analyzing glucose molecules using the electromagnetic property by spectral means could get more complicated at the sensor end and for the in-vivo conditions for continuous monitoring. However, electrochemical transduction is more feasible, measuring electron affinity proportional to the concentration of the analyte or its byproduct [28]**.**

When it comes to electrochemical transduction, this could be achieved in three ways[28]:

1. Measuring electric potential – Potentiometric transduction.
2. Measuring electric current - Amperometric transduction.
3. Measuring electric impedance or conductance– Conductometric transduction.

The sensing element in potentiometric ion sensors is a membrane including ion-selective molecular receptors or receptor sites in a solid material typically used to obtain the potential signal for specific ions concerning analyte species. This membrane is generally an ion-selective electrode placed in the solution of the analyte of interest along with the reference electrode with a constant potential. When no current is passed through them, the relative concentration of the analyte generated or consumed is proportional to the potential draw between the two electrodes. However, Glucose is charge neutral and does not readily dissociate into ions for this approach.

Amperometric enzymatic sensors are based on enzymes catalyzing oxidation-reduction reactions and involve an inorganic molecule as a coreagent. Oxygen is the natural coreagent in such responses, but artificial coreagents in more advanced designs can substitute it. Amperometric transduction is best suited to affinity-based sensors provided that an electrochemically active compound is attached to the recognition product P (from Eq.(1)). It detects the concentration of the analyte at fixed potential by measuring current.

Electrochemical impedance measurements provide broad information about the physicochemical processes occurring in an electrochemical cell, such as ion migration, charge distribution at the electrode/electrolyte interface, and the velocity of the electrochemical reaction[28]. It consists of an electrode and a sensitive layer. When a sensitive layer comes in contact with the analyte of interest, a change in impedance between the electrode and sensitive layer could be measured proportional to the analyte. This method, however, is much easier to fabricate. They are not suited for in-vivo applications but are used extensively in external or in-vitro applications.

2.1. CHOICE

From the transduction methods mentioned above, the amperometric system is scalable and works best both in in-vivo and in-vitro applications. Change in a chemical reaction with respect to an enzyme can be easily read by the current drawn through it.

Chemical ⟶ Current

- measures electron affinity.
- Best suited for an enzymatic reaction involving oxidation/reduction.

Also, by making a nano biosensor [27]**:**

fM ⟵ mM

- Sensitivity increases (Can determine up to fM change in concentration of an analyte in the medium)
- Increases Form factor

2.2. AMPEROMETRIC SENSOR

This type is a suitable transduction method when coupled with an enzymatic reaction involving oxidation/reduction steps, such as catalyzed by oxidase and dehydrogenase enzymes. A general scheme for the oxidase-catalyzed reaction is given in Eq.(2), where S is the substrate and P is the product.

$$S+O_2+2H^+ \xrightarrow{\text{oxidase}} P+H_2O_2 \qquad (2)$$

2.2.1. WORKING

The setup consists of three electrodes: an Auxiliary or Counter electrode (CE), the reference electrode (RE), and the working electrode (WE) immersed in a medium in which the analyte should be recognized. This setup measures the concentration of an analyte with a current response at a fixed potential. Voltage is applied between two electrodes during measurements (as shown in Figure 4) and the current $A_{Meas.}$ It is measured corresponding to the concentration of an analyte in the medium[29]. By passing negligible or no current through the RE, the Working

electrode potential is stabilized. CE passes all the current back through WE and makes the circuit a closed loop.

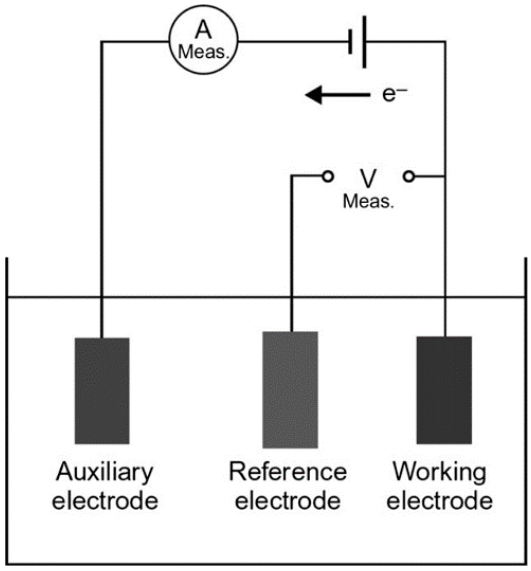

Figure 4: Three-electrode setup for amperometry [29]

Let's consider Glucose as an example (from [22]). From Eq.(2), Glucose is the substrate (S), and Gluconic acid is the product (P). In this case, the detection is through H_2O_2 formation. Which is:

$$\text{Glucose} + O_2 \xrightarrow{\text{Oxidase } (GO_x)} \text{Gluconic acid} + H_2O_2 \quad (3)$$

$$H_2O_2 \xrightarrow{+500\text{mV vs. RE}} O_2 + 2H^+ + 2e^- \quad (4)$$

$$2H^+ + \frac{1}{2}O_2 + 2e^- \longrightarrow H_2O \quad (5)$$

At the WE surface, H_2O_2 is detected When biased with +0.6V, which results in Eq. (3) and, in turn, the sufficient voltage at anodic WE vs. the RE (in this case +500mV) leads to oxidation, refer to Eq.

(4), while at CE, Eq. (5) balances the current flow by reducing as shown in Figure 5.

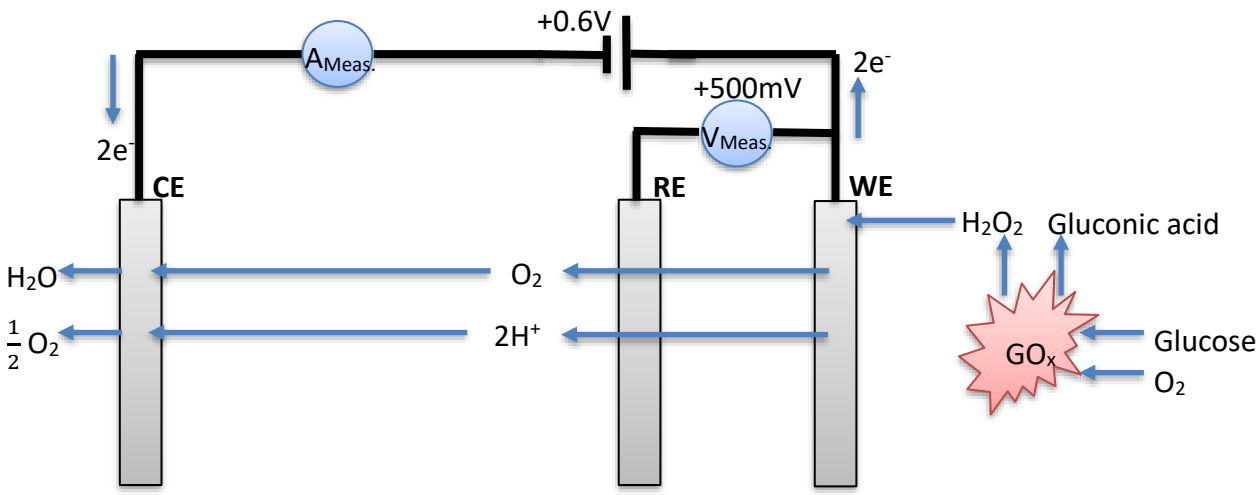

Figure 5: Pictorial representation of the working of amperometric setup concerning glucose sensing

However, in [22], it is mentioned that at bias +0.6V, other common interferents, which are electroactive substances present in the IF, such as ascorbic acid (AA) and uric acid (UA), hinder the detection of hydrogen peroxide, by oxidizing and contributing to the current, often noticed as noise current leading to false glucose reading. The excess oxygen involved in the reaction concerning Glucose must be limited at the WE surface to avoid saturation effects w.r.t the glucose concentration range. Consequently, additional precautions were made in [22] at the WE to ensure correct operation and selectivity by depositing selectively permeable membrane Nafion and perm-selective membrane polyurethane on top of three electrodes during fabrication.

2.2.2. CATEGORIES

Based on the evolution of the technologies used in glucose detection, enzyme oxidase based Amperometric sensors are divided into three generations[28]:

A. **First-generation Amperometric sensor:** electrochemical monitoring of either oxygen depletion or hydrogen peroxide formation.

B. **Second-generation Amperometric sensor:** oxygen is replaced by artificial e^- acceptor (redox mediators) in the biocatalytic layer.

C. **Third-generation Amperometric sensor:** direct e^- transfer from reactant species to electrodes.

A. FIRST-GENERATION AMPEROMETRIC SENSOR

These are the most straightforward amperometric transduction utilizing oxidase as a catalyst

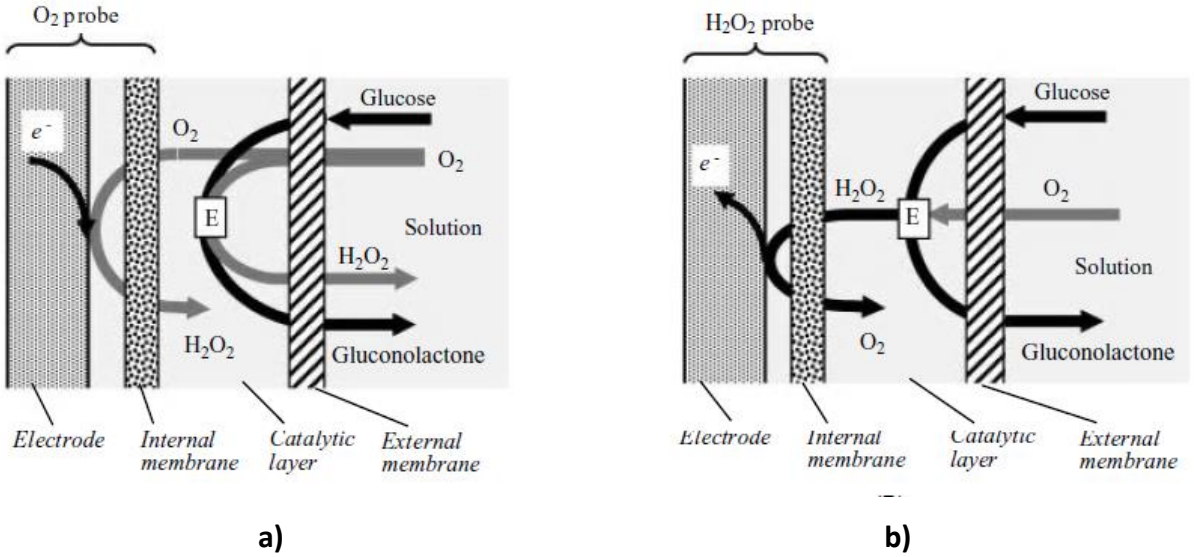

Figure 6: Configurations of first-generation glucose detection using amperometry a) with O_2 probe and b) with H_2O_2 probe [28]

in the reactions, transduction relies on detecting natural cosubstrates such as oxygen or the bi-product, H_2O_2. In the first case, Enzyme E is entrapped between the oxygen probe and the IF with another semipermeable or external membrane, as shown in Figure 6 a). Immobilization (keeping enzyme intact) of the enzyme is achieved by having an internal membrane. Glucose, along with dissolved O_2, diffuses into the enzyme layer. Apparently, in this layer, Glucose in contact with E or GOx (Glucose Oxidase) and dissolved O_2 undergo a reaction as mentioned in Eq.(3). Residual O_2 diffuses further into the internal membrane to the O_2 probe, where reduction occurs. With an O_2 probe as a WE, a decrease in O_2 concentration is detected relative to the response in the absence of substrate [28].

In the second case, Enzyme E is entrapped between the H_2O_2 probe and the IF with another semipermeable or external membrane, as shown in Figure 6 b). Immobilization of the enzyme is achieved by having an internal membrane. Glucose and dissolved O_2 diffuse into the enzyme layer, forming H_2O_2 as the byproduct from Eq.(3). H_2O_2 further diffuses to the H_2O_2 probe or anodically polarised electrode, where it is oxidized to water, leading to the current proportional to H_2O_2 and, in turn, proportional to the glucose concentration.

A.1. LIMITATIONS

- **The dependency of O_2 concentration:** Uncontrolled variations in the oxygen concentration with the sample leads to a false reading from the O_2 probe, especially in the in-vivo conditions**.**
- **The dependency of interferents:** Interferents like UA, AA, and acetaminophen lead to the measurement's biased current. That is, it leads to a false reading of the current. Hence requires one or more layers at the external membrane to sort out interferents entry to the enzymatic layer.

B. SECOND-GENERATION AMPEROMETRIC SENSOR

This type relieves a few limitations of the first-generation amperometric sensor, particularly the dependency on oxygen supply. It is achieved using an artificial electron acceptor called 'Mediators' as an oxygen substitute. Here transduction is performed by stepwise transfer of e^- using intermediate relays (enzyme and mediators). The reaction scheme for such a sensor is shown in Figure 7, where grey arrows indicate intermolecular electron transfer and dark arrow means actual chemical reaction. The reaction scheme follows the below equations [28]:

$$S + E_O \rightleftharpoons ES \longrightarrow P + E_R \quad (6)$$

$$E_R + mM_O \longrightarrow E_O + mM_R \quad (7)$$

$$M_R \longrightarrow M_O + ne^- \quad (8)$$

Where S is the substrate, E_0 is the enzyme active site, ES represents the substrate in contact with the enzyme active site, P is the product, ER is the reduced form of the enzyme, M_O is the mediator species, and MR is the reduced form of the Mediator. The subscript 'O' represents species in their oxidized state, and 'R' represents the species in their reduced state.

At the beginning of the reaction, from Eq. (6), substrate S, in contact with enzyme active site E_O forms product P by liberating an e^-. That is, an e^- is transferred from E_O to S, whereas the enzyme is converted into its reduced form E_R. Next, following Eq. (7), the oxidized form of enzyme E_O is regenerated by the e^- transfer to the electron acceptor or mediator M_O, forming a reduced form of Mediator M_R. In the end, the resulting reduced form of Mediator M_R undergoes further reaction (from Eq. (8)) to regenerate the oxidized form of mediator M_O at the electrode interface, making a stepwise e^- transfer from substrate to the electrode with enzyme and electrode as an intermediate relay. Figure 7 shows the conventional flow of e- from the substrate to the electrode.

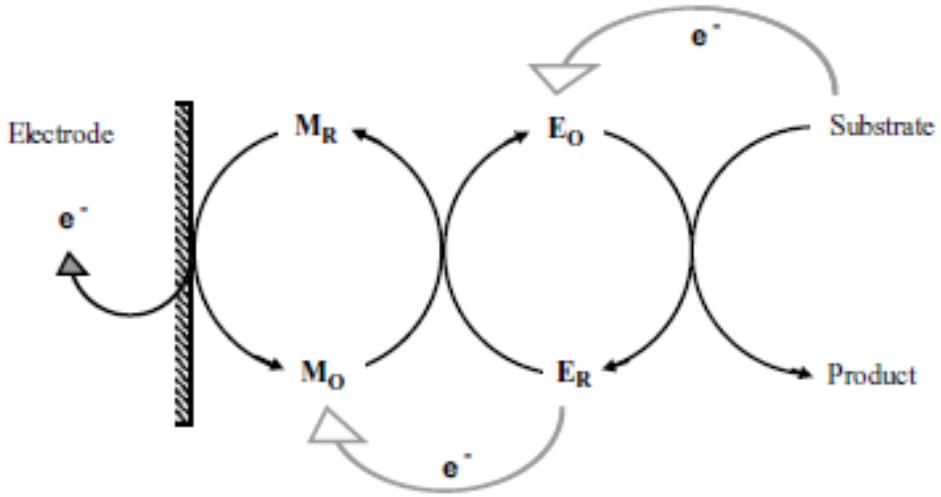

Figure 7: Schematic representation of reactions involved in second-generation amperometric sensor

B.1. LIMITATIONS

- **Hydrogen ions interfere**: From Eq. (2), glucose reaction with enzyme includes hydrogen ions which hinder e^- transfer to the Mediator, resulting in false or no current reading during measurements.
- **Dissolved oxygen interferes:** Instead of reduced enzyme E_R transferring e^- to the Mediator (follow Eq. (7)), dissolved oxygen competes and gives rise to a bias in the response current. It requires additional immobilization techniques that are perm-selective only to enzymes hampering dissolved oxygen excess.

C. THIRD-GENERATION AMPEROMETRIC SENSOR

These are the most advanced amperometric transduction involving direct electron transfer between the prosthetic group (a non-protein group still a part of a protein, for example, flavin) of an oxidoreductase species and electrode. This type simplifies sensor configuration and doesn't depend on cosubstrates or mediators [28]. Different approaches have been proven successful and are mentioned in the below sections.

C.1. USING CONDUCTING ORGANIC SALT ELECTRODES

Conduction through organic salt, TTF.TCNQ salt with direct e^- transfer from redox enzyme is discussed in [30]–[32]. TTF (Tetrathiafulvalene) is an e^- donor species, and TCNQ (Tetracyanoquinodimethane) is an e^- acceptor species, as in Figure 8. The TTF.TCNQ compound is

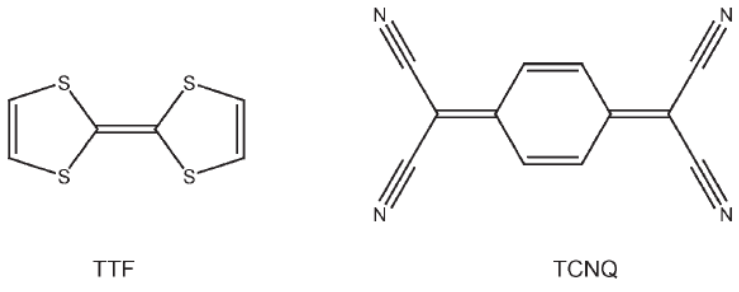

Figure 8: Chemical structure of TTF and TCNQ [31]

an oxidoreductase species. This compound is a segregated stack of cations and anions of donor and acceptor species or a planar molecule with delocalized π orbitals extending above and below the molecular plane. It belongs to the class of charge transfer compounds with semiconductor properties.

A schematic of TTF.TCNQ salt integrated with poly-pyrrole (PPy) in glucose sensing is shown in Figure 9 a) The Pt electrode and TTF.TCNQ compound is crosslinked using a strong electrostatic attraction between the charged protein molecule (poly(pyrrole)) and the intrinsic electric charge at the electrode surface or simply strong adsorption at the solid surface. Enzyme active site E (glucose oxidase/GOx) is immobilized in the BSA-glutaraldehyde membrane (buffer). It follows Eq. (2) reactions, with S being a substrate and P product.

The only difference concerning other methods is that the partial e^- transfer occurs from E to Pt electrode via the $(PPy)_{ox}$/TTF.TCNQ complex through its crosslinked branches without mediator species (no additional oxidation/reduction steps involved, as seen in second-generation sensors). Figure 9 b) shows the STM image of TTF.TCNQ single crystal salt, where the topography indicates multilayers of TTF.TCNQs, stacked on top of each other in the direction of 'a', and conduction occurs from right to left or in the direction of 'b' in the form of a charge density wave pattern collectively carrying the electric current. Thus, leading to the flow of current proportional to the concentration of the substrate.

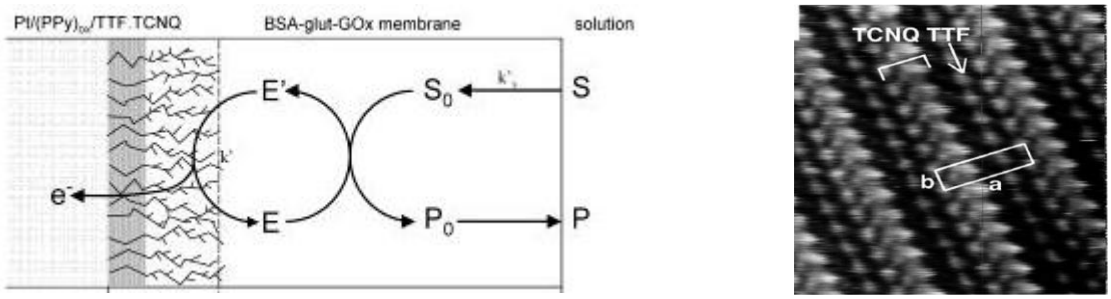

a) **b)**

Figure 9: Glucose sensing using conducting organic salt a) Schematic [31]*, b) STM image of TTF.TCNQ compound [31]*

C.1.1. LIMITATION

- From [30], it is noted that the geometry of the enzyme-salt-electrode system at the molecular level is not optimal, which renders the e^- transfer relatively inefficient when compared to nanomaterials (see section C.2. Using nanomaterials)
- From [30], [33], it has a small potential window of operation -0.2V vs RE to +0.4V vs RE (RE used here is Standard Calomel Electrode, SCE). For potential more negative to -0.2V vs RE, the $TCNQ^-$ is released to the solution, and for potential more positive than +0.4V vs RE, $TCNQ^-$ is oxidized to neutral TCNQ water-soluble and remains on the electrode surface.

C.2. USING NANOMATERIALS

This type relieves limitations of sensing using conducting organic salt electrodes. In the previous section, it was noted that the enzyme-salt-electrode system of the organic salt electrode type at the molecular level is not optimal with an inefficient e^-transfer. However, from [28], [33], [34], it is clear that close control of the sensing architecture of the biocatalytic layer could be achieved by integrating the active enzyme with nanoparticles to obtain direct e^- transfer between the active enzyme and the electrode.

C.2.1. USING GOLD NANOPARTICLES

In [33]–[35], glucose sensing is achieved utilizing gold nanoparticles. e^- transfer occurs between the active enzyme and the electrode directly by wiring both employing Au nanoparticles. A schematic with the only working electrode (WE) is shown in Figure 10 [35]. Here Au nanoparticle is functionalized with a FAD derivative (ligand conjugated Au nanoparticle), allowing interaction with glucose oxidase. The enzyme active site/GOx is attached to ligand conjugated Au nanoparticles. On the other hand, this is attached to the WE for amperometric operation. This bridge is established using dithiol-modified spacers. Thus, an organic nanowire is established between the electrode and the conjugated Au nanoparticle. At the enzyme active site, Glucose

undergoes reaction w.r.t Eq.(2). Thus, e^- transfer occurs, resembling the concentration of Glucose, which is proportional to the current flow.

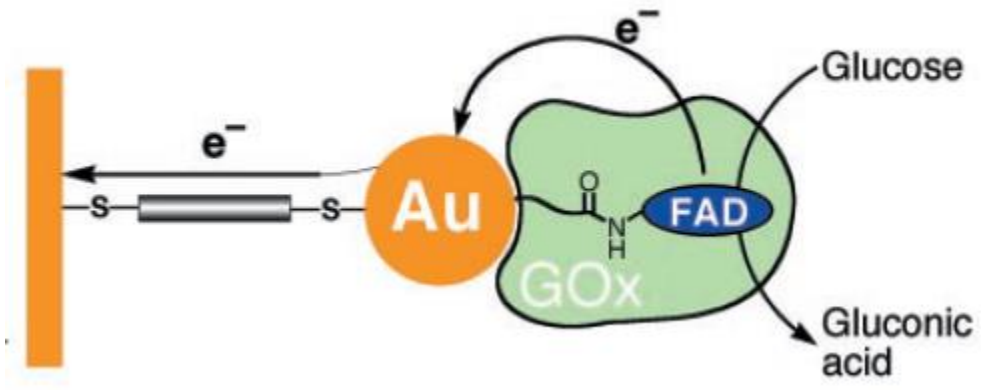

Figure 10: Schematic of glucose sensing using Au nanoparticles [35]

C.2.2. USING CARBON NANOTUBES

In [28], [36], glucose sensing is achieved using carbon nanotubes (CNT). Direct e^- transfer between the electrode and the active enzyme is achieved by wiring both using a carbon nanotube.

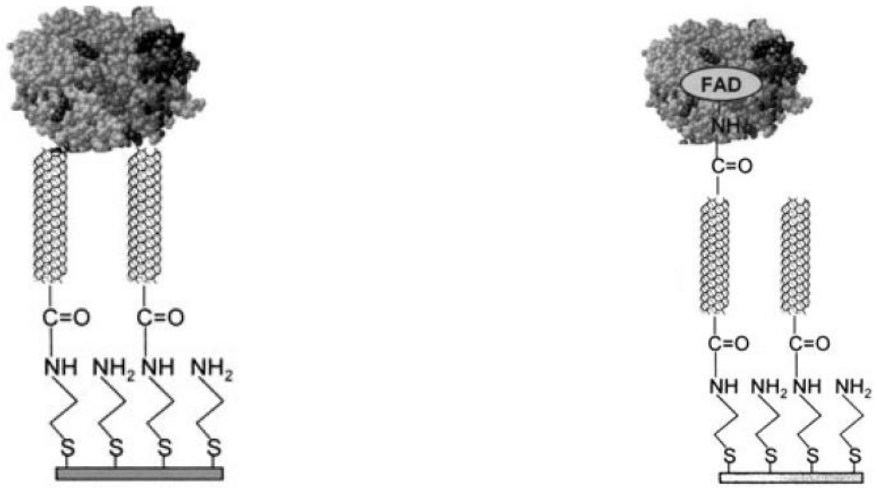

a) **b)**

Figure 11:Schematic of glucose sensing using carbon nanotube with a) enzyme directly attached to CNT b) enzyme wired to CNT through FAD derivative [36]

A schematic of the same with the only working electrode (WE) is shown in Figure 11. Here electrode is modified with a self-assembled monolayer of cysteamine and is aligned to the electrode surface with shortened single-walled carbon nanotube (SWNT). Two approaches are employed to wire enzymes in [27], [35]. In the first case, the enzyme (glucose oxidase) is covalently attached to the ends of the aligned nanotube, shown in Figure 11a). In the second case, the FAD prosthetic group is attached to the ends of the aligned carbon nanotube and with the enzyme around the surface-immobilized FAD, shown in Figure 11b). In both cases, at the enzyme active site, Glucose undergoes reaction w.r.t Eq.(2), and the e^- proportional to the Glucose concentration is transferred through the wiring, resulting in the equivalent current for sensing.

In conclusion, both methods (using Au nanoparticles and CNT) are characterized by high-speed electron transfer and respond linearly to glucose concentration even at a higher concentration range (mM range). However, from [34] and [36], it is clear that wiring using Au nanoparticles showed an electron transfer rate of 5000 s^{-1} and that CNT showed a maximum of 9 s^{-1}.

CHAPTER 3. DESIGN AND FABRICATION

Our design is as discussed in section 2.2.1. WorkingIt consists of WE, CE, and RE Pt metal as a part of a three-electrode amperometric approach in the sensing area shown in Figure 12 a). Although third-generation devices with Au NPs looked promising from the literature, It was decided to fabricate and analyze the first-generation devices with H_2O_2 detection as the fabrication process technology for the former has more than 70% similarities to the design mentioned in the latter. Thus, minimizing the cost and complexity of the design to understand the behavior of the test devices. Individual chips designed on a silicon wafer were 5mmx5mm. The sensing area with three different Pt metal features to act as electrodes were connected to bond pads using Pt metal wire routes. Bond pads were of 430µm x 430µm dimensions to achieve connection to the external closed loop. Border markings and design numbers were fabricated with metals while implementing technology in the process flow. A cross-sectional schematic of the individual chip after fabrication in the clean room and post-processed with functioning RE(IrO_x) and enzyme active site (GO_x) is shown in Figure 12 b). An intermediate Si_xN_y layer was designed to insulate the Pt metal electrodes from the underlying conductive Si substrate. An additional layer of Si_3N_4 was designed to isolate the three metal electrodes and to avoid edge effects during post-processing.

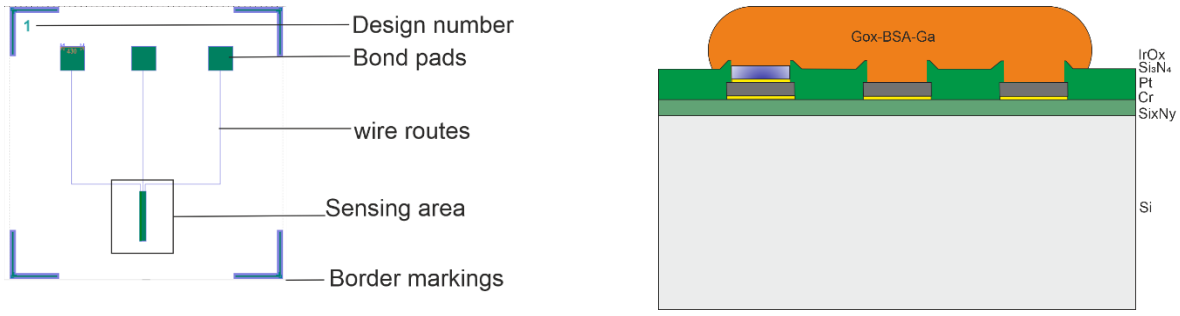

(a) (b)

Figure 12: A pictorial representation of a) design on-chip, b) Cross-section of the design in the sensor area on-chip fabricated in a cleanroom and post-processed.

Electrodes were deposited with different dimensions and spacing between them, as shown in Table 2. Also, different electrode geometry or configurations were used, as shown in Figure 13. Design 1, 2, and 3 have dimensions and geometry configurations similar to [21], [22].

Design 1 (µm)		**Design 1_1 (µm)**		**Design 1_2 (µm)**	
RE	905x35	RE	455x45	RE	455x45
WE	900x30	WE	450x40	WE	450x40
CE	900x30	CE	450x60	CE	450x60
Spacing	10	Spacing	10	Spacing	20
Design 2 (µm)		***Design 2_1 (µm)***		**Design 2_2 (µm)**	
RE	240x85	RE	105x45	RE	105x45
WE	325x70	WE	100x40	WE	100x40
CE	260x60	CE	120x60	CE	120x60
Spacing	10	Spacing	10	Spacing	20
Design 3 (µm)		***Design 3_1 (µm)***		**Design 3_2 (µm)**	
RE	175x75	RE	340x135	RE	340x135
WE	170x70	WE	335x130	WE	335x130
CE	170x70	CE	335x130	CE	335x150
Spacing	10	Spacing	10	Spacing	20
Design 4 (µm)		***Design 4_1 (µm)***		**Design 4_2 (µm)**	
RE	175x75	RE	100x250	RE	100x250
WE	170x70	WE	245x95	WE	245x95
CE	170x70	CE	245x135	CE	245x135
Spacing	10	Spacing	10	Spacing	20

Table 2: Represents the design dimension of the three-electrode setup used in this work

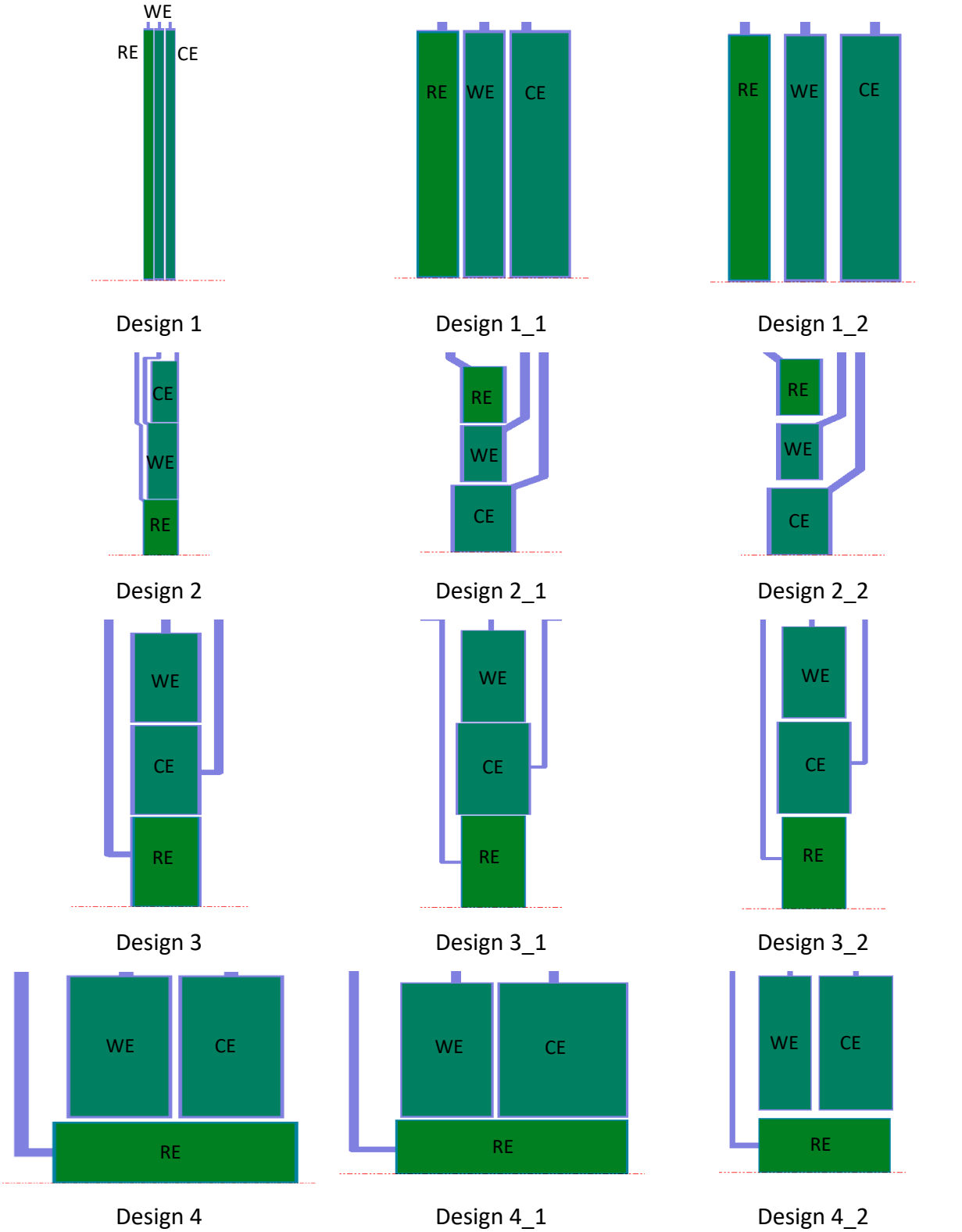

Figure 13: Represents the design geometry used in this work. Light green (RE), blue(wire routes), electrode connecting the centre wire (WE) and the rightmost (CE)

Where Light green represents RE, blue represents wire connection, the electrode connecting to the center wire is WE, and the rightmost is CE. CleWin software was used to create a mask layout on a 5-inch mask. Dice lines and chip alignment marks were taken care of, as shown in Figure 14.

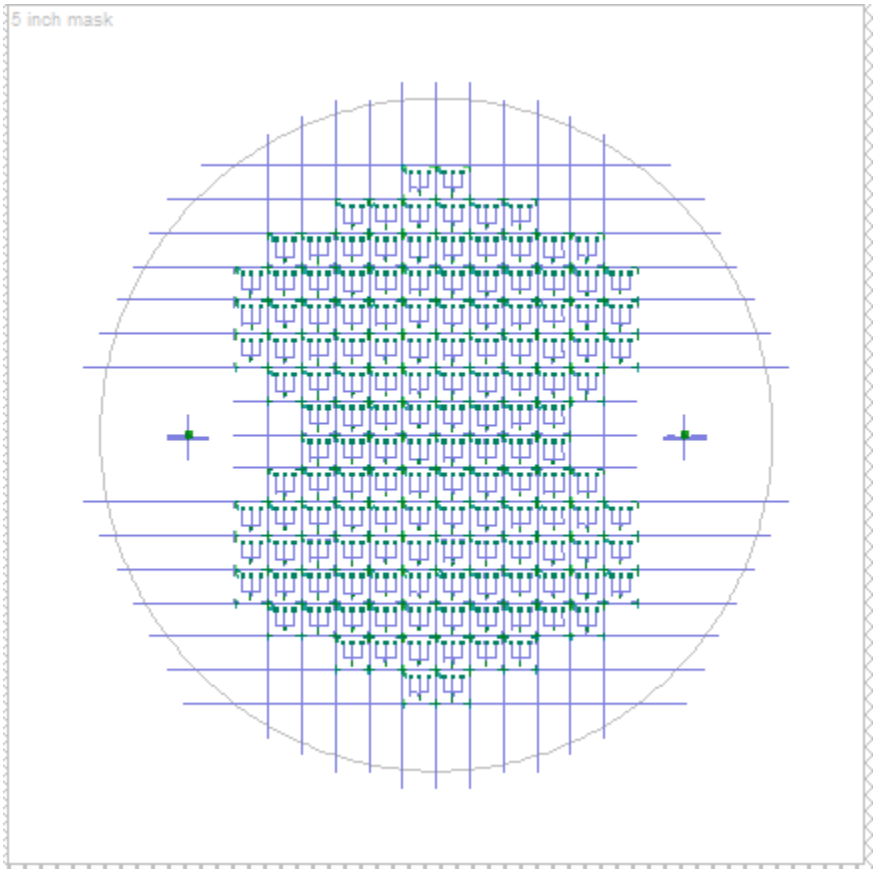

Figure 14: 5-inch Mask designed for the fabrication using CleWin

3.1. PROCESS FLOW FOR THE FABRICATION OF THE TEST DEVICE

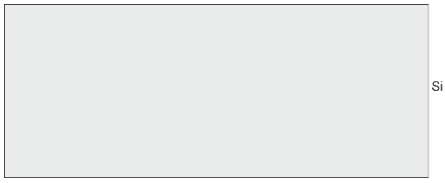

(a) Silicon wafer

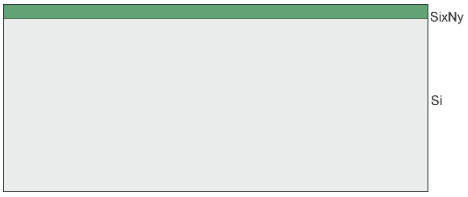

(b) LPCVD silicon-rich Si_xN_y

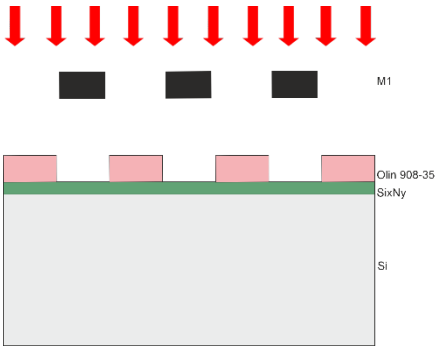

(c) Photoresist and patterning for lift-off 1

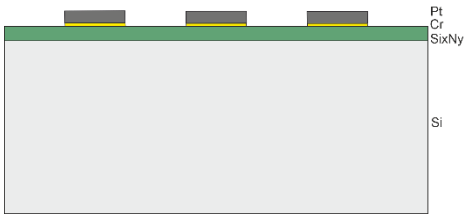

(d) Sputtered Cr/Pt and lift-off

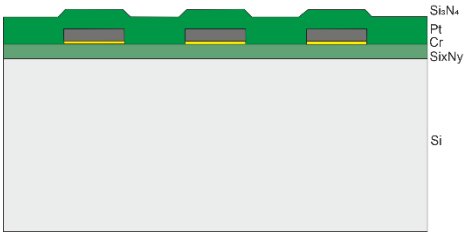

(e) PECVD Si_3N_4

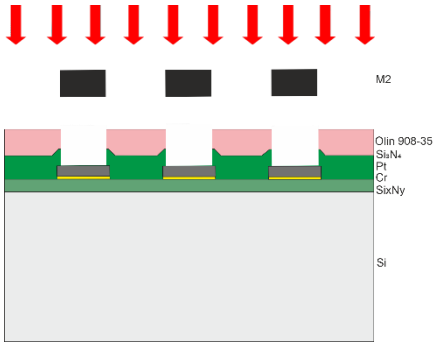

(f) Plasma etching of Si_3N_4

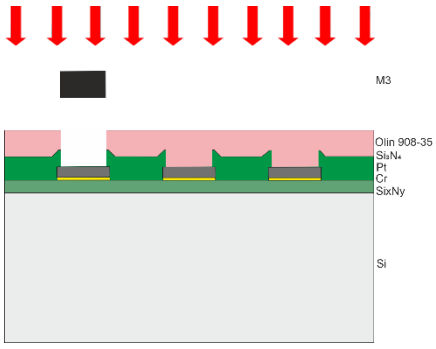

(g) Photoresist for patterning lift-off 2

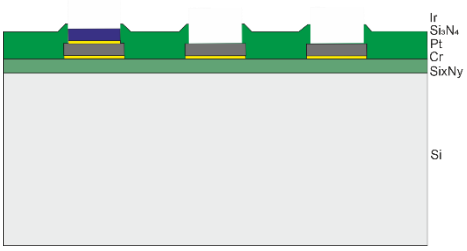

(h) Sputtering Cr/Ir and lift-off

Figure 15: Overview of the process flow used in the test device fabrication in the cleanroom before post-processing.

Device fabrication was done at MESA+ Institute. Figure 15 (a) represents the Si substrate; the first low-stress silicon-rich Si_xN_y was deposited using LPCVD, shown in Figure 15 (b). Negative photoresist Olin 908-35 of thickness 3.5µm was spin-coated and exposed with Mask 1 (M1) to form desired trenches for the electrode deposition, Figure 15 (c). 5nm Cr followed by 100nm of Pt was deposited in the trenches using sputtering and lift-off as shown in Figure 15 (d), refer to APPENDIX A. Second layer of Si_3N_4 of thickness 500nm was grown using PECVD, shown in Figure 15 (e). Later, nitride openings to expose Platinum electrodes, Si_3N_4, were etched using Mask 2 (M2) by plasma etching, as in Figure 15 (f). Further, 5nm Cr followed by Ir of thickness 100nm was deposited by sputtering at a speed of 15nm/min for 6:45 (min: sec) and lift-off techniques using mask 3 (M3), as shown in Figure 15 (g) and (h) respectively. Refer to APPENDIX A for the detailed process flow. Figure 16 shows the schematic of the cross-section of the design fabricated in the cleanroom before post-processing. Further, Chapter 4 discusses functionalizing the RE by oxidizing the Ir metal and activating the sensor by depositing the enzyme active site.

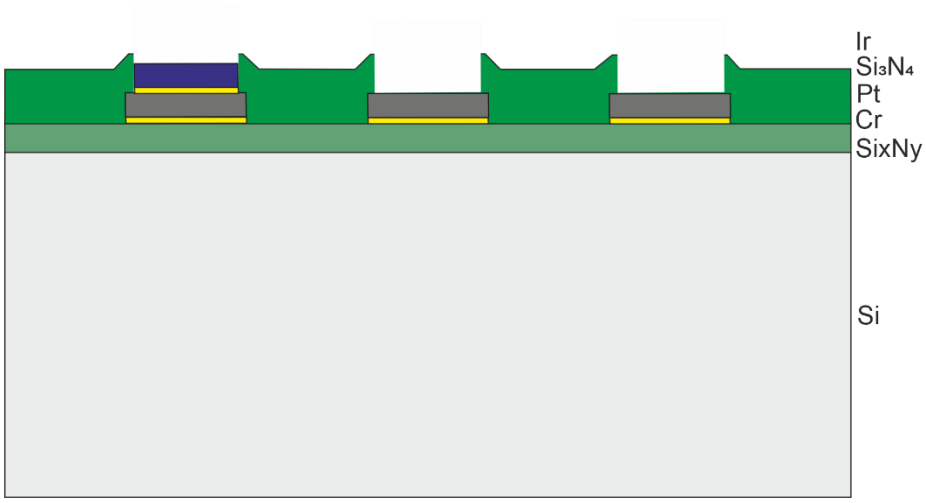

Figure 16: A cross-section of design on-chip fabricated in a cleanroom before post-processing.

3.2. PROCESS FLOW FOR THE FABRICATION OF THE FUTURE DEVICE

The design for the future device in the sensing area is discussed in section C.2.1. Using gold nanoparticles A schematic of which is shown in Figure 17. Compared to the test device used in this project, It utilizes underlying Au metal instead of Pt to form the underlying WE and CE. Additional functionalization of WE with spacer-FAD conjugated Au nanospheres is required to achieve the direct e^- transfer.

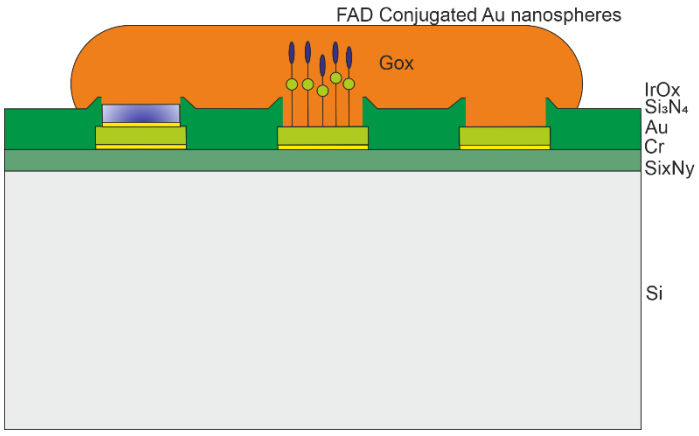

Figure 17: Schematic representation of the future device with Au NPs after post-processing

The process flow for the fabrication of the future device is shown in Figure 18. Figure 18 (a) represents the Si substrate; the first Si_xN_y layer could be deposited using LPCVD technology, shown in Figure 18 (b). A negative photoresist Olin 908-35 can be spin-coated and exposed with Mask 1 (M1) to form desired trenches for the electrode deposition, shown in Figure 18 (c). An adhesive layer of Cr followed by Au can be deposited in the trenches using sputtering and lift-off as shown in Figure 18 (d), refer to APPENDIX B. Second layer of Si_3N_4 can be grown using PECVD, shown in Figure 18 (e). Later, nitride openings to expose Platinum electrodes, Si_3N_4, can be etched using Mask 2 (M2) by plasma etching, as in Figure 18 (f). Further, an adhesive layer of Cr followed by Ir can be deposited using sputtering and lift-off technique using Mask 3 (M3), Figure 18 (g) and (h). To functionalize the WE spin-coat, the photoresist and pattern the trench using Mask 4 (M4), as shown in Figure 18 (i).

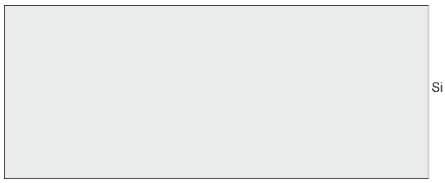

(a) Silicon wafer

(b) LPCVD silicon-rich SixNy

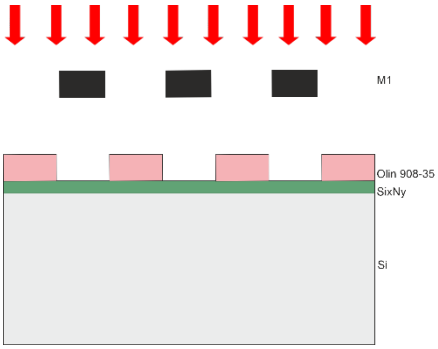

(c) Photoresist and patterning for lift-off 1

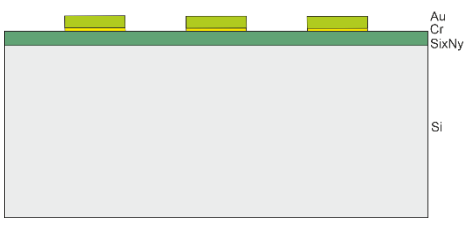

(d) Sputtering of Cr/Au and lift-off

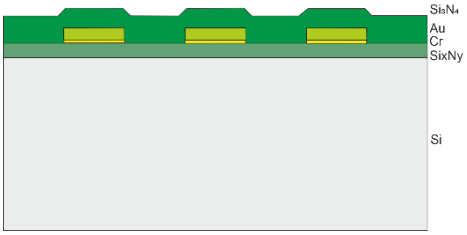

(e) PECVD Si_3N_4

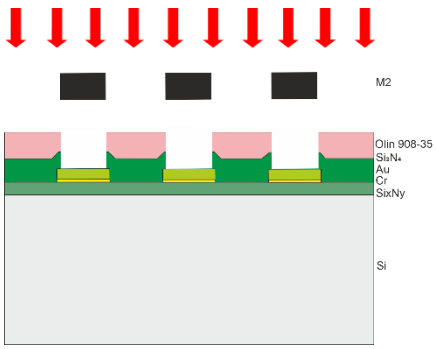

(f) Plasma etching of Si_3N_4

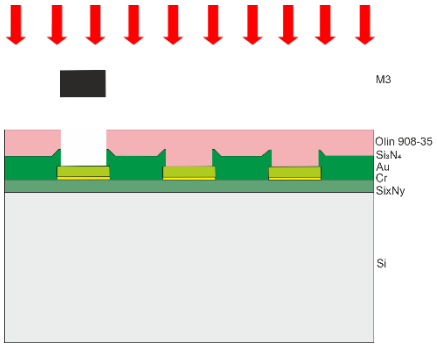

(g) Photoresist and patterning for lift-off 2

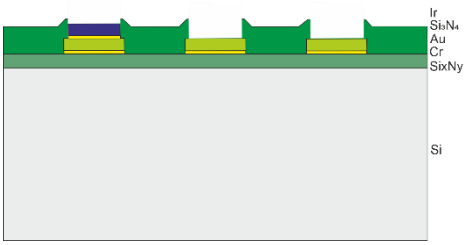

(h) Sputtering of Cr/Au and lift-off

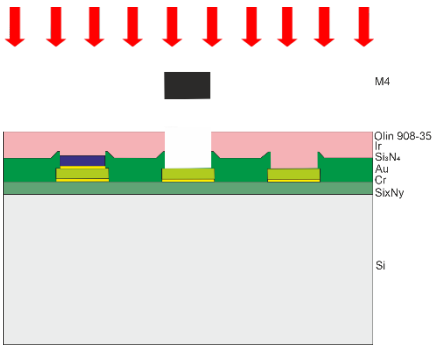

(i) Photoresist and patterning to functionalize WE

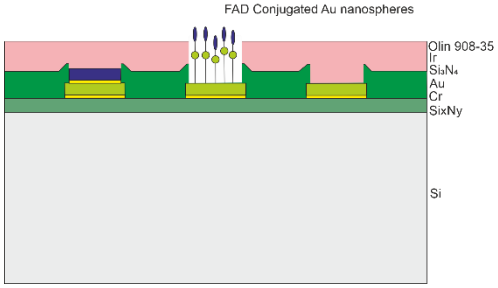

(k) Attaching FAD conjugated AU NPs with spacer bridge

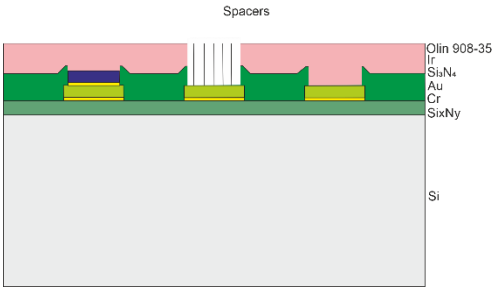

(j) Spacer bridge formation

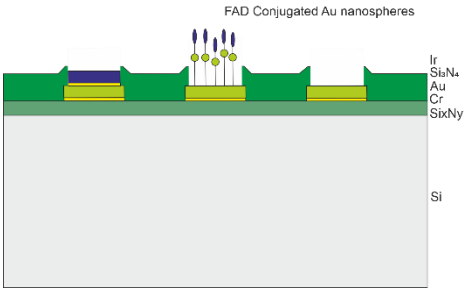

(l) Remove photoresist

Figure 18: Overview of the process flow for the fabrication of the future device in the cleanroom without post-processing

To form a spacer bride at the WE surface, immerse the device from Figure 18 (i) in a 2.5mM solution of 1,4-BDMT in dichloromethane overnight and wash it with dry ethanol. Spacers should be self-assembled [35], as shown in Figure 18 (j). However, care must be taken to perform this step without light to avoid photooxidation. To wire ligand (FAD) conjugated Au nanosphere, commercially available FAD conjugated Au nanosphere can be self-assembled or wired to spacers overnight [35], as shown in Figure 18 (k),(l). Refer to APPENDIX B for the detailed process flow. Figure 19 a) shows the schematic cross-section of the device after cleanroom processing. Further, post-processing can be done to functionalize the RE by oxidizing Ir following the same process flow used in chapter 4. To activate the sensor, deposit the enzyme active site by shaking the device in 4mg mL^{-1} apo-GOx in 0.1M phosphate buffer, at pH 7.0 for 4hr at 25°C and 12hr at 4°C. Rinse by shaking it for 1hr in 0.1M PBS, at pH 7.0 and 0°C [33], [35]. A schematic cross-section of the same after post-processing is shown in Figure 19 b).

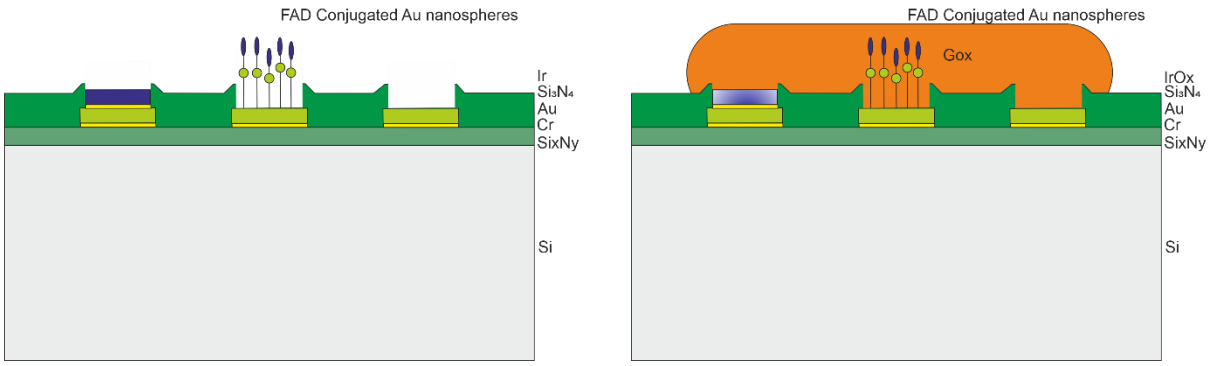

(a) (b)

Figure 19: Cross-section of the future device with AU NPs a) before post-processing b) after post-processing

CHAPTER 4. POST-PROCESSING

For the experiments or deposition outside the cleanroom, the fabricated chips were mounted onto PCB using super glue, as shown in a schematic and practical as in Figure 20 (a) and (b), respectively. Au wire bonding of type wedge bonding was done between the bond pads of the chip and PCB for the connection. Figure 20 (c) provides the parameters for the same, where bond 1 and bond 2 represents the parameters at which Au wire was wedge bonded on the bond pads of chip and PCB, respectively.

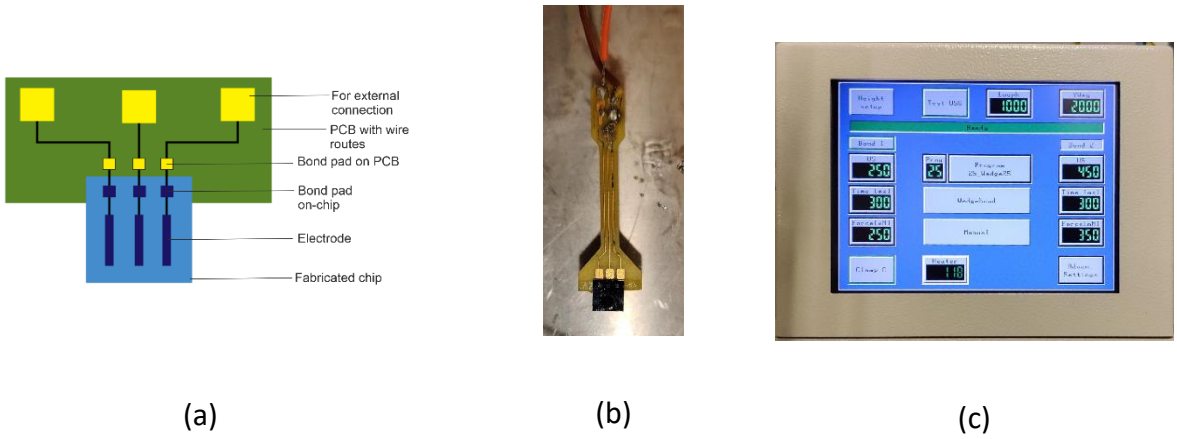

(a) (b) (c)

Figure 20: Designed chip mounted on PCB: (a) Schematic, (b) In practice, and (c) Showing wire bond parameters

4.1. TO FUNCTIONALIZE RE

To fix the potential at the WE, RE plays a vital role, as explained in section 2.2. Amperometric sensor standard macroscopic RE cannot be used in these miniaturized devices. Instead, a much more reliable pH-sensitive reference electrode or Quasi-reference electrode (Q-RE) needs to be implemented. These characterize a short lifetime (several days) compared to the conventional macroscopic RE. When standard REs like Ag/Agcl is implemented as a miniature device, they can lead to toxicity in the medium and are unsuitable for in-vivo applications, as they can be

inflammatory. Hence, reliable devices are Q-REs with IrOx with good stability and relatively high charge storage capacity (CSC) [21], [22].

There are many techniques to oxidize Ir films and are not limited to electrodeposited IrO_x film (EIROF), Thermal IrO_x film (TIROF), Sputtering IrO_x film (SIROF), and activated IrO_x film (AIROF). However, EIROF includes expensive starting materials, and the setup is complex. TIROF requires a high-temperature environment. SIROF requires high vacuum equipment and accurate control of Ar and O_2 flow. AIROF has simple fabrication methods and reproduces relatively high CSC [37].

The AIROF technique with the Cyclic Voltammetry method was used to oxidize the Ir microelectrode on-chip. PBS (Phosphate Buffered Saline) at pH 7.4 was purchased from Sigma-Aldrich, a Palm Sens device as a Potentiostat, Pt wire as a CE electrode, and a standard Ag/Agcl electrode for external reference. Figure 21 shows the setup to achieve Q-RE on chip (To oxidize Ir) utilizing cyclic Voltammetry (CV).

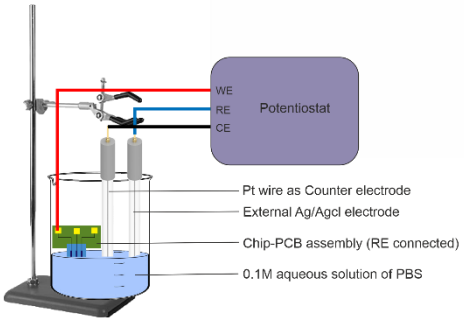

Figure 21: Experimental setup to functionalize Q-RE

Ir electrode on the chip is connected to the WE terminal of the potentiostat (red). External Pt wire is used as the CE. It is connected to the CE terminal of the potentiostat (Black). External standard Ag/Agcl is used as RE and is connected to the RE terminal of the potentiostat (Blue), as shown in Figure 21.

The cycling potential of Ir between hydrogen (HER) and oxygen evolution extremes (OER) between +0.95V to -0.75V (A difference of 1.7V much higher than 1.23V required for electrolysis of water) was used. Ir on-chip as WE, external Pt wire as CE, and external Ag/Agcl as RE was immersed in a solution containing 0.1M Phosphate-buffered Saline (PBS) deaerated prior to CV. The potential was swept at the rate of 200mV/s for 30 scans or activation cycles [21], [22].

The cyclic voltammogram curve of current vs. potential indicates the two regions' oxidation and reduction, as shown in Figure 22. Anodic reaction represents positive current values due to oxidation, and cathodic reaction represents negative current values due to reduction. Precisely, the voltammogram's Anodic and cathodic current peaks ipa and ipc represent the oxidation and reduction peak.[38]. The area under the peaks gives charge storage capacity (CSC).

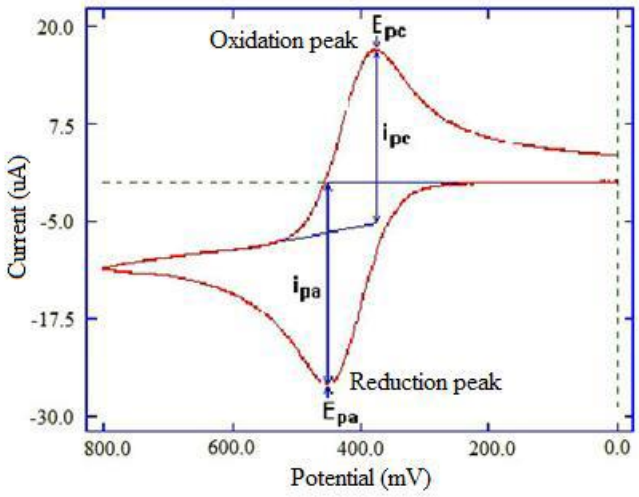

Figure 22: cyclic voltammogram showing reduction and oxidation peaks [38]

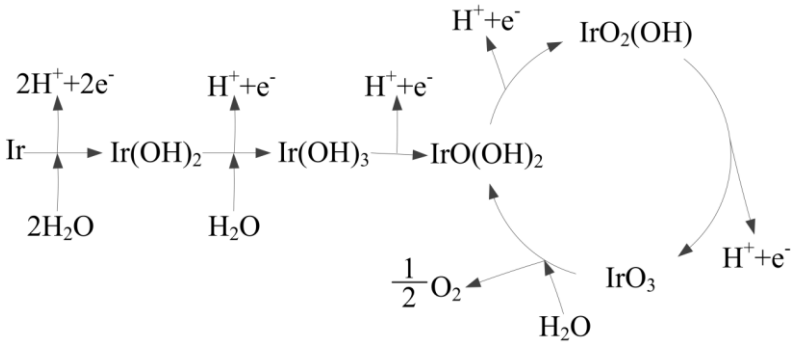

(9)

From [37], Eq (9) represents the oxide formation of Ir. With the increase in the activation cycle, sputtered Ir on microelectrode oxidizes to $Ir(OH)_2$, Ir(II) oxide, as shown in eq(10). Further, Ir(II) triggers the eq(11) oxidizing Ir(II) to $Ir(OH)_3$, Ir(III) oxide. Furthermore, Ir(III) triggers the eq(12) oxidizing the Ir(III) to $IrO(OH)_2$, Ir(IV) oxide. Ir(IV) oxide becomes a reversible reaction with further activation cycle. Figure 23 a) and b) represent the schematic of Ir and IrO_x before and after cyclic Voltammetry.

$$Ir + 2H_2O - 2e^- = Ir(OH)_2 + 2H^+ \quad (10)$$

$$Ir(OH)_2 + H_2O - e^- = Ir(OH)_3 + H^+ \quad (11)$$

$$Ir(OH)_3 - e^- = IrO(OH)_2 + H^+ \quad (12)$$

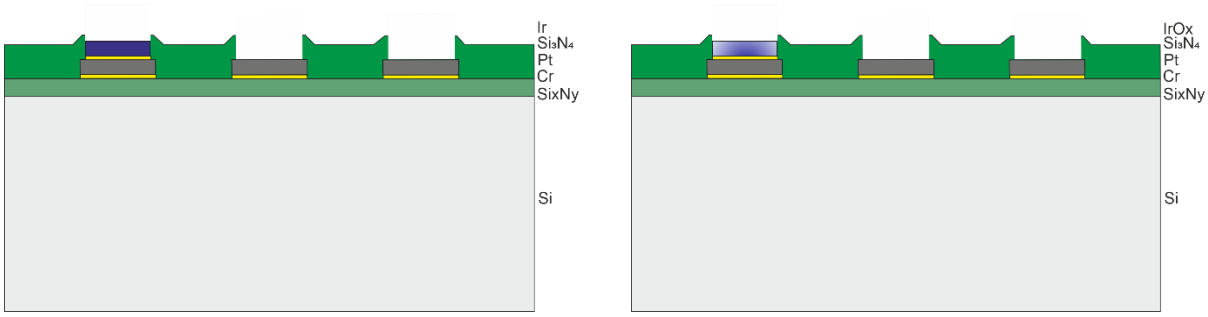

(a) (b)

Figure 23: Cross section of a chip showing a) Ir before CV and b) IrOx after CV

4.1. TO FUNCTIONALIZE WE

As discussed in section 2.2., the measurement of Glucose in our test device is an enzymatic reaction by reading equivalent H_2O_2 formation.

To activate the WE by enzyme-rich active site: Bovine serum albumin (BSA), Glutaraldehyde (GA) grade I, 25% and Glucose oxidase (GOx, aspergillus niger VII) were purchased from Sigma-Aldrich.

With the help of a pipet gun, an aqueous solution of 100nL of 3wt% Gox and 3wt% BSA was drop cast onto the sensor region. Later, an aqueous solution of 100nL of 2wt% GA was drop cast on top, and each layer was allowed to dry for 45min. BSA is a buffer, and GA is a crosslinker holding the enzyme [21], [22], as shown in Figure 24

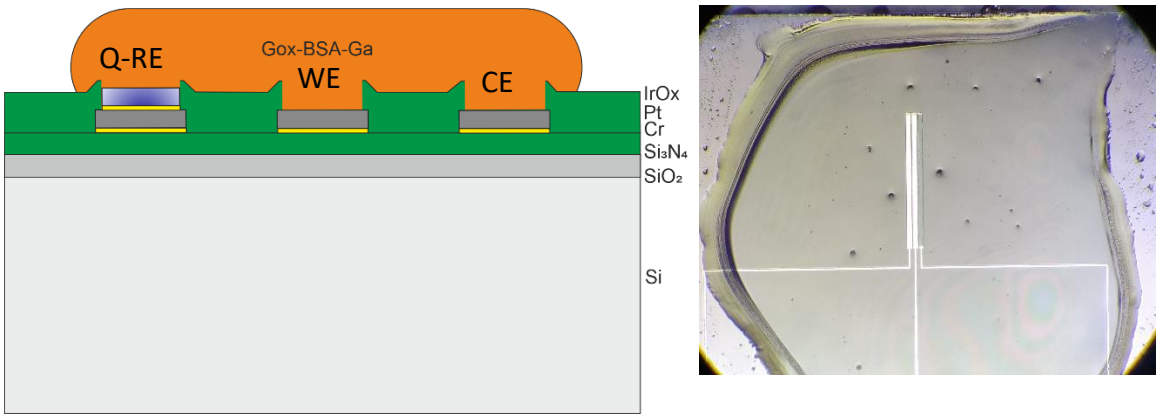

Figure 24: a) Cross section of the test chip showing Q-RE, WE, CE, and enzyme active site, b) showing sensing area covered with enzyme active site

CHAPTER 5. EXPERIMENTAL SETUP FOR GLUCOSE MEASUREMENT

An amperometric three-electrode setup is used to test the fabricated sensor, as mentioned in section 2.2. Amperometric sensorA WE, CE, and RE terminal on-chip are connected to WE, CE, and RE of the potentiostat, respectively, as shown in Figure 25.

PBS (Phosphate Buffered Saline) at pH 7.4 and d-(+)-Glucose were purchased from Sigma-Aldrich.

The design mounted on PCB is immersed in 0.1M PBS, applying +0.5V vs. RE and a bias +0.6V, and left for an hour before adding d-(+)-Glucose in 50mg/dL increments. The results are discussed in Chapter 6.

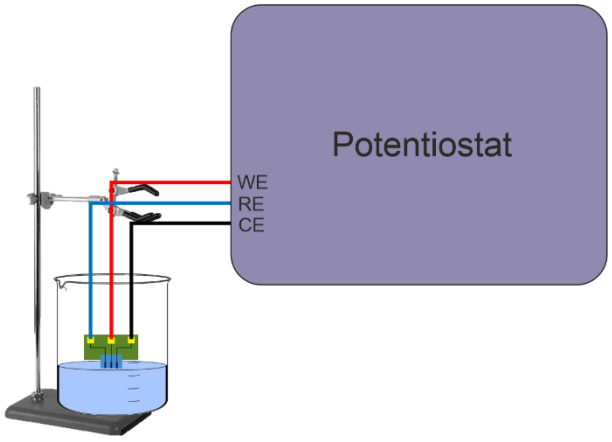

Figure 25: Experimental amperometric setup to test the designed sensor

Further, Figure 26 and Figure 27 represent the glucose concentration measurements as in [21] and [22] for comparing results in Chapter 6.

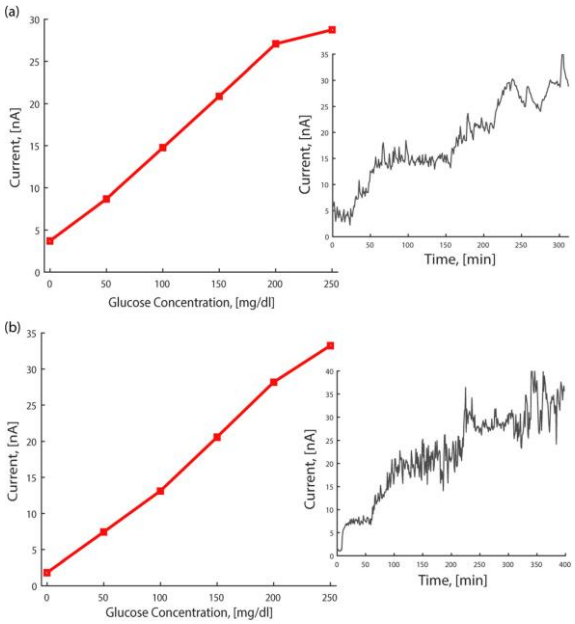

Figure 26: In-vitro measurements of the glucose sensor and inset: chronoamperometry, at bias +0.6V a) with +0.5V vs. Q-RE microelectrode and b) with external Ag/Agcl electrode [21]

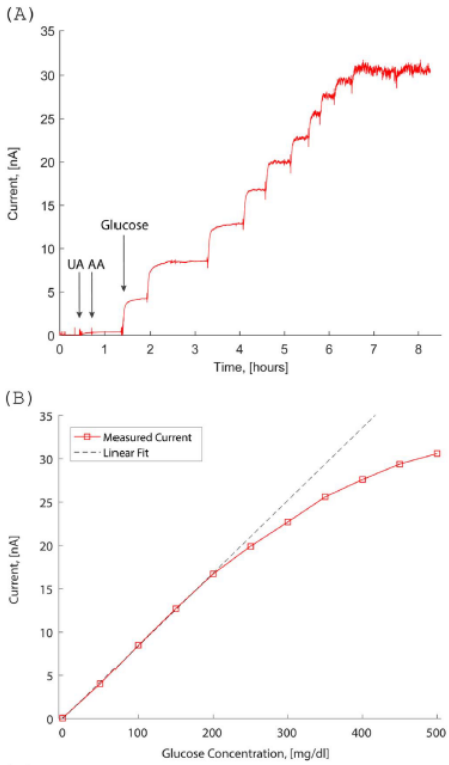

Figure 27: In-vitro measurements of glucose senor a) showing the Chronoamperometry measurements vs. the Q-RE in PBS buffer at an incremental concentration of Glucose, 50mg/dL and AA, UA electroactive interferents of 100 µM each b) linear fit of the curve (a) vs. Q-RE [22]

CHAPTER 6. RESULT

Glucose amperometric measurements of the fabricated sensor design showed a small peak when 50mg/dL of Glucose was incremented in a 0.1M PBS buffer, as shown in Figure 28. It did not provide the desired outcome compared to the results shown in Figure 26 and Figure 27. PSTrace 2.5.2.0 was used to perform the measurements in the PalmSens potentiostat.

To understand the failure of the sensor, the Open circuit potential (OCP) of the fabricated micro RE was done using voltammetric measurements. The OCP of 0.2V vs. external Ag/Agcl electrode was observed initially and exponentially reached zero within a minute. However, in [21], [22] a stable OCP of 0.28V was observed for four days. But, from Figure 29 a) and b), Ir sites on the fabricated design showed a color change, indicating the formation of IrOx with electrochromic behavior in the physical observation.

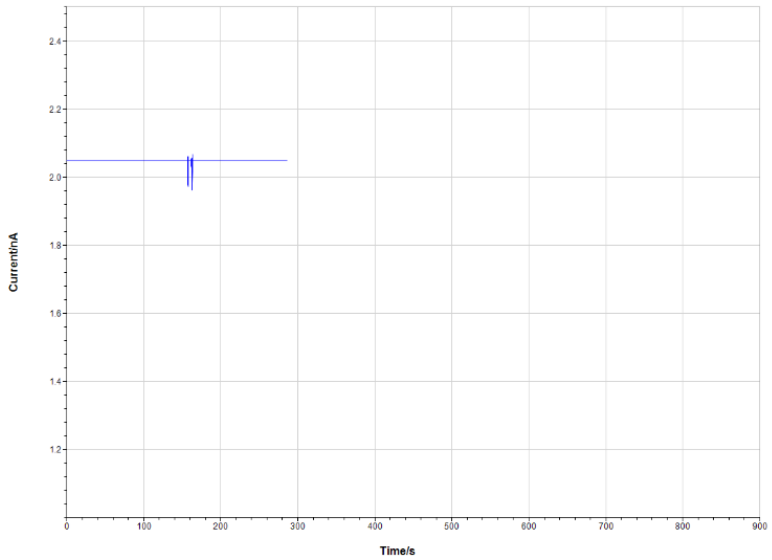

Figure 28: In-Vitro amperometric measurement of the fabricated sensor showing a change in current vs. time when a Glucose with 50mg/dL is dissolved in the 0.1M PBS buffer

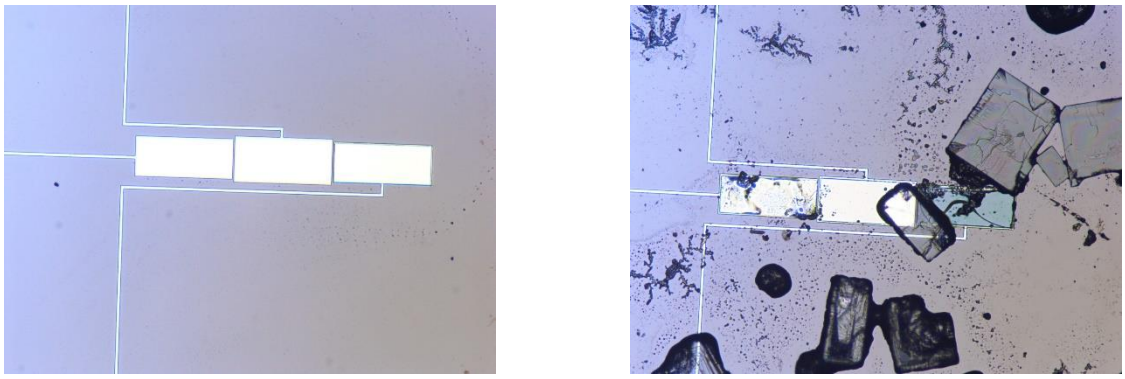

(a) (b)

Figure 29: Microscopic image of the sensor design a) before and b) After functionalizing the fabricated RE in the post-processing

CV of the Ir site to form IrO_x did not show significant peaks compared to Figure 22 to indicate the oxidation Of Ir. CV was performed with a total of 30 scans or activation cycles, as shown in Figure 30 a) and the 1st, 10th,20th, and 30th activation cycles, as shown in Figure 30 b).

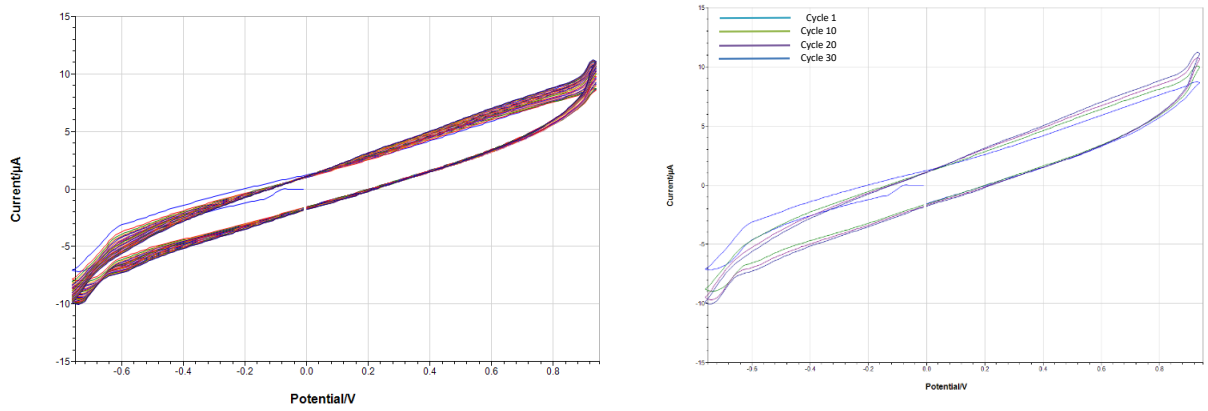

(a) (b)

Figure 30: Cyclic Voltammogram of Ir site to form IrOx used in post-processing a) showing all curves b) Showing Curve 1, 10, 20 and 30th scan

Further, to confirm the oxidation state of Ir sites. XPS analysis was performed at MESA+ Institute. Software used were Compas for XPS control, PHI Multipack V9.8.0.19 for data reduction, CasaXPS VAMAS V2.3.14 for prost processing and NIST Database V1-1 for simulation of electron spectra for surface analysis. Survey scans were made to see the gross overall atomic content of the surface layer except for the elements H and He with concentration as low as 1% pollutants can

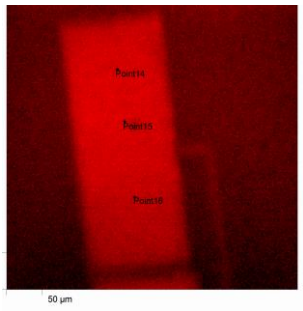

(a)

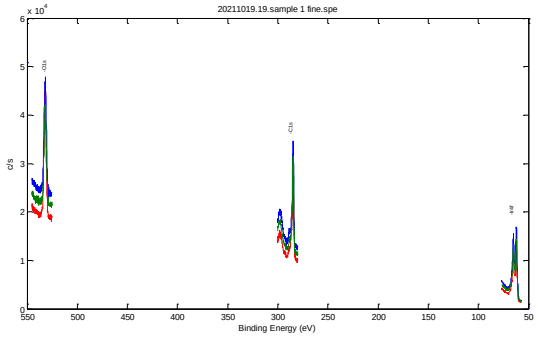

(a.1)

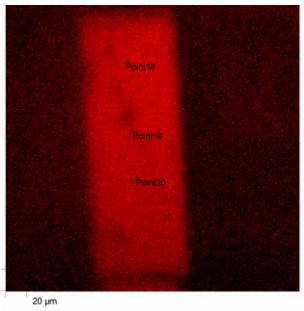

(b)

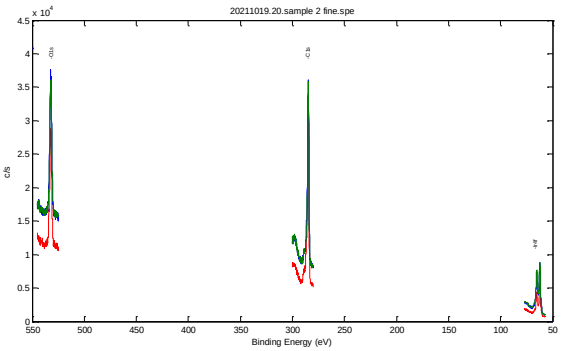

(b.1)

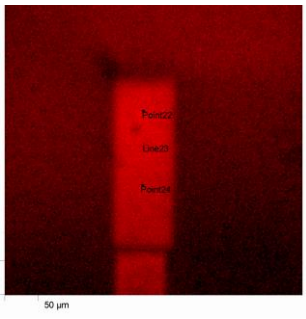

(c)

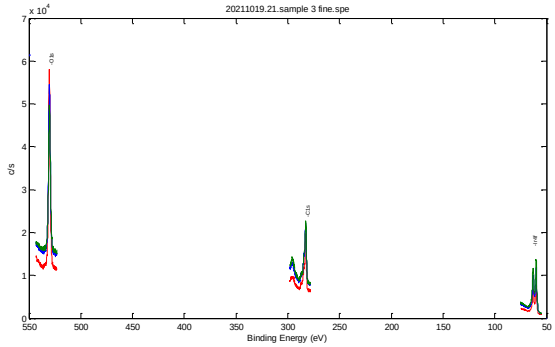

(c.1)

Figure 31: Three different samples a, b and c showing Ir and Oxides presnt in the core spectral analysis in a.1, b.1 and c.1 respectively in the O1s and Ir4f spectra

show up. Three different design samples were tested in the spectral range of -5eV to 1345eV of binding energy, refer APPENDIX C. The spectral shift due to sample charging (photoelectron emitted from the sample surface leave positive charge on the sample and as a result it builds up charge shifts in the binding energies of the emitted electrons) was corrected with the standard uncharged value of carbon in C1s spectra with binding energy of 284.8eV. The core spectral analysis at Ir sites showed the presence of Oxides and Ir in the O1s and Ir4f spectra respectively on the Ir sites, as shown in Figure 31. The O1s spectra as shown in **Error! Reference source not found.**, clearly indicates three oxidation states of Ir with OH bonds with three peaks of emitted photo electrons in the binding energy levels of oxide. This confirms the Ir(II), Ir(III) and Ir(IV) hydoxides on the Ir site.

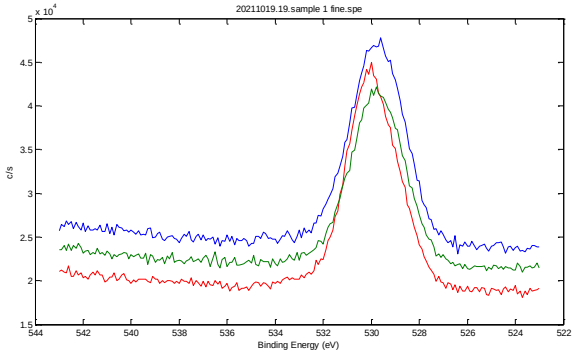

(a)

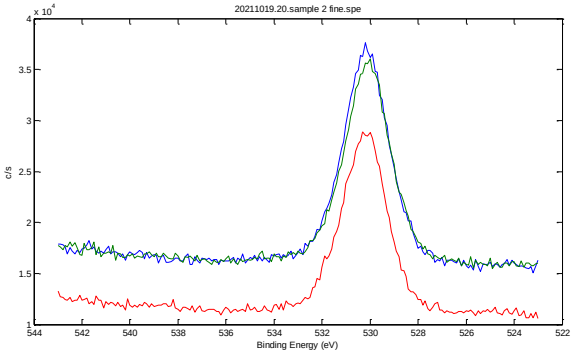

(b)

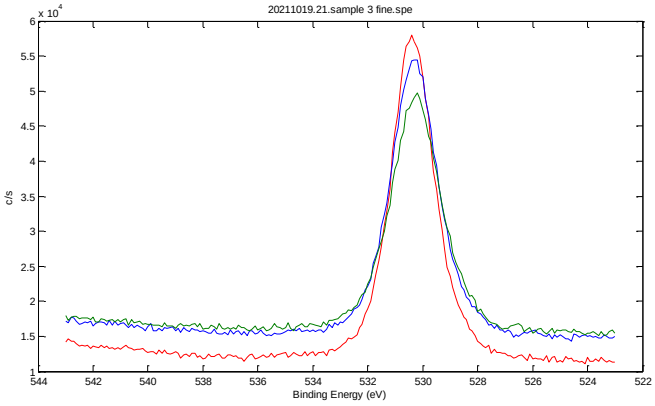

(c)

Figure 32:: O1s spectra of the XPS analysis of three samples a, b and c showing three oxidized states of photoelectrons emitted In C/s with respect to the binding energies of oxide.

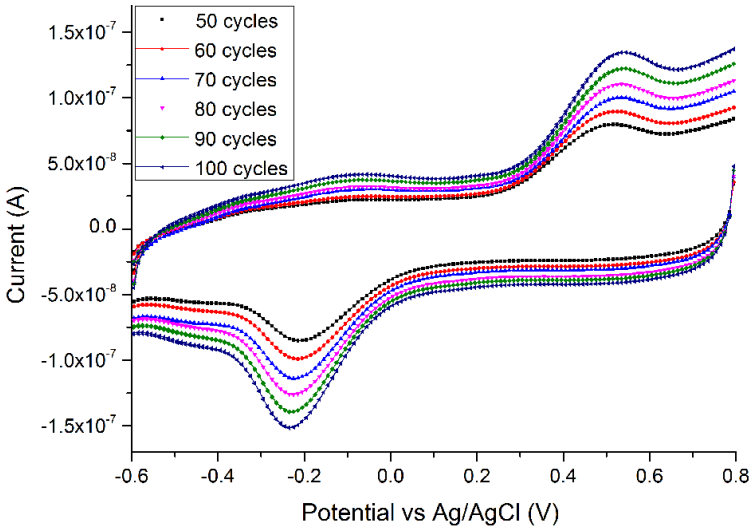

Figure 33: CV of sputtered microelectrodes for 100 activation cycles [37]

From [37] activation cycles greater than 50 in CV provides the significant peaks, as shown in Figure 33. This is because, eq(10) occurs on the Ir microelectrode site to form Ir(II) oxide. However, this Ir(II) oxide is further consumed by eq(11) to form Ir(III) oxide leaving behind bare ir microelectrode surface. Later , Ir (III) oxide is consumed in eq(12) to form Ir(IV) oxide. This goes on until the whole electrode surface is covered by Oxide. Hence, it can be concluded from the XPS analysis and [37] that higher activation cycles are required to form rough and porous IrO_x layer making it permeable to water and ions. Due to the significant peaks relatively high CSC could be obtained.

CHAPTER 7. CONCLUSION AND RECOMMENDATION

In conclusion, an amperometric enzymatic sensor design, assuming it could be implanted into the dermal region of the skin to measure glucose concentration in the IF (Interstitial Fluid) between the body cells was studied. The fabrication process flow for the third-generation amperometric sensor with Au nanoparticles was made to achieve a high response sensitivity. However, since more than 70% of this design coincides with the first-generation devices (with H_2O_2 detection) and the expensive material requirements and complexity, it was decided to fabricate the first-generation devices and analyze their behavior. Different geometry of the design with varied dimensions to examine its working with the three-electrode amperometric approach were made. Part of the fabrication was done at the MESA+ institute and was later post-processed in the external laboratory to functionalize the sensor. PBS buffer solution was used with the cyclic voltammetric approach to form a Pseudo-reference metal microelectrode by oxidizing Ir metal on-chip using the AIROF technique. Later the sensor was activated using enzyme active site. The fabricated sensors did not behave as expected due to the failure to attain pseudo reference as a part of its design. Due to the lack of activation cycles in developing IrO_x on top of Ir microelectrodes to act as a pseudo reference, the final glucose measurements did not provide desired results.

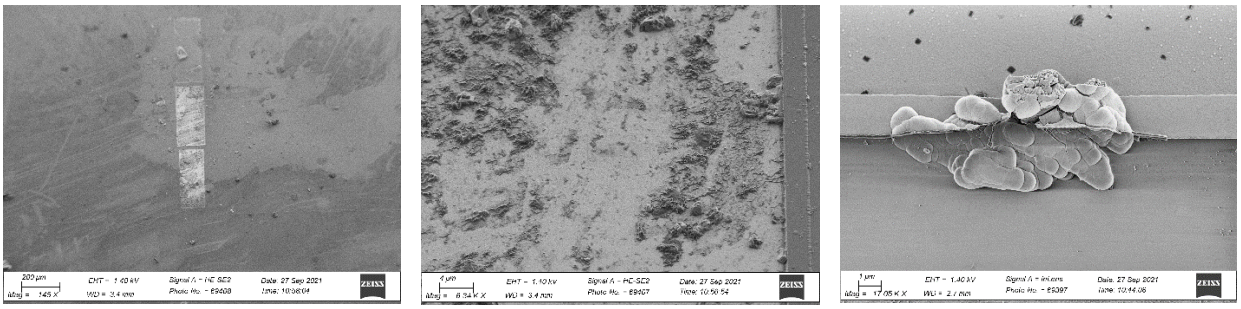

Figure 34: HRSEM images showing Impurities or pollutants on-chip after CV

As a recommendation for the future, increase the activations cycles in CV while functionalizing the Ir sites, refer [37]. OCP measurement data are not included in this report. It, is essential to observe the OCP measurements of the integrated Pseudo-RE electrode, to understand the stability of the sensor, as IrO_x is pH dependent. From Figure 34, there are lot of pollutants on-chip. Thoroughly rinse chips with H_2O after CV and before drop casting enzyme on the sensing area. From [39] include a polyurethane membrane to increase the linearity in measuring glucose concentration, specifically at higher concentration of glucose (mM). Include Nafion membrane to interrupt electroactive interferents such as AA and UA from entering to the enzyme active site, as shown in Figure 35. Vary the layer thickness of the above-mentioned membrane and choose the optimum layers to use in the physiological application. Alternately, fabricate the advanced device with Au nanospheres.

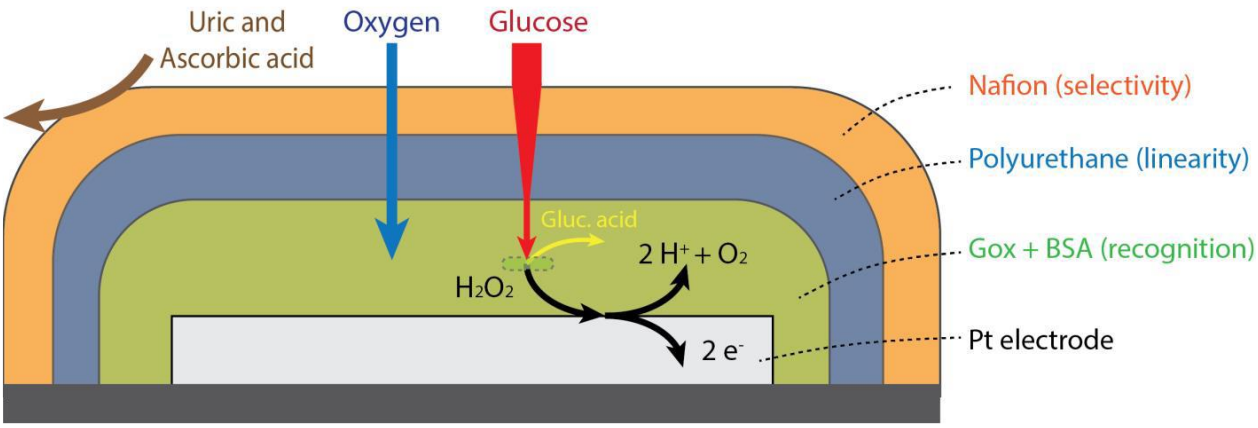

Figure 35: Schematic of WE showing addition membranes to avoid electroactive interferents and to increase linearity.

APPENDIX A

Process flow for the fabrication of the test device is as follows:

- Prepare a Si substrate or use Si wafer

- Grow SixNy using LPCVD (thickness is not critical here)

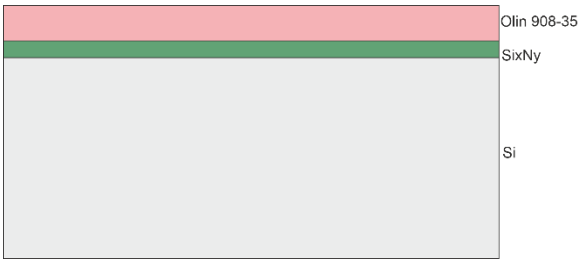

Beginning of lift-off process (1) to deposit Pt electrodes

- Spin-coat a lift-off photoresist (Olin 908-35)
- Soft bake

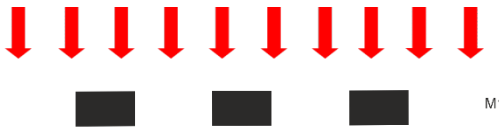

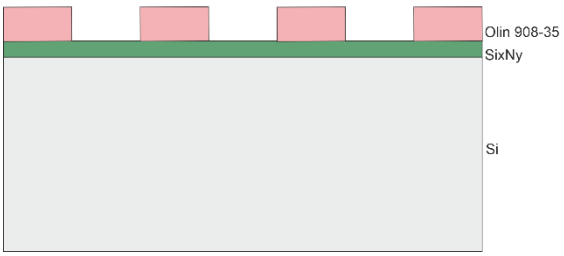

- Expose with the Mask (M1) to pattern trenches, to deposit electrode metal (Pt)

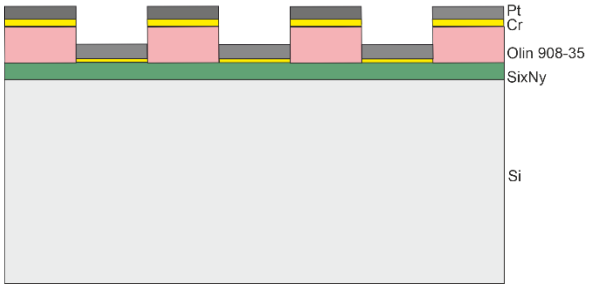

- Deposit an adhesive layer Cr by sputtering
  (Alternatively, Ti can be used)
- Deposit metal, Pt by sputtering

- Strip off the photoresist (Olin 908-35)

<u>End of lift-off process (1)</u>

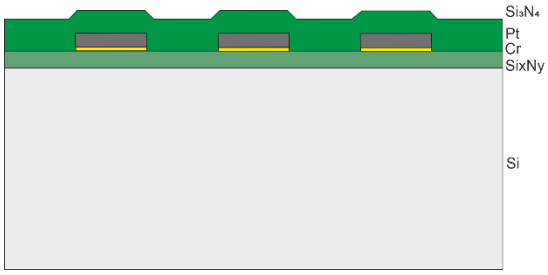

- Deposit a layer of Si_3N_4 using PECVD

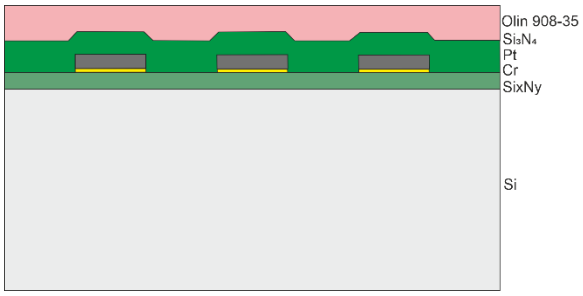

<u>To make openings to the buried electrode under Si_3N_4</u>

- Spin-coat and soft bake photoresist (Olin 908-35)

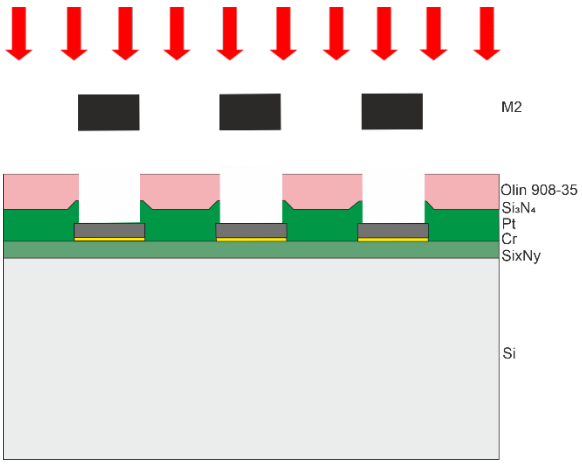

- With the help of IBL or plasma etching and mask (M2)
- Pattern the trenches in the photoresist layer and further beyond to the Si_3N_4 layer until it reaches the buried Pt metal.

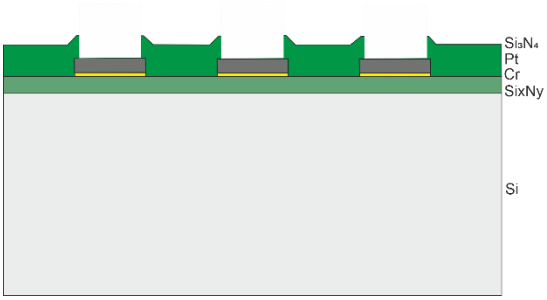

- Strip off the photoresist

End of the formation of the Working electrode (WE) and counter electrode (CE)

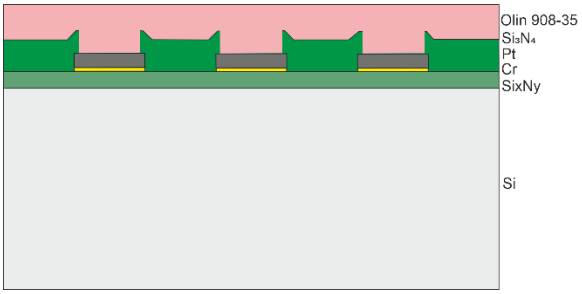

Beginning of the lift-off process (2) to deposit Ir

- Spin-coat and soft bake lift-off photoresist (Olin 908-35)

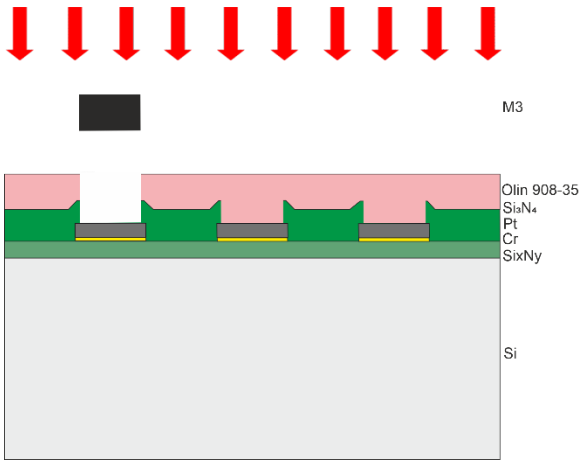

- Expose with the mask (M3)
- Pattern the photoresist to form trench at the target site to deposit Ir

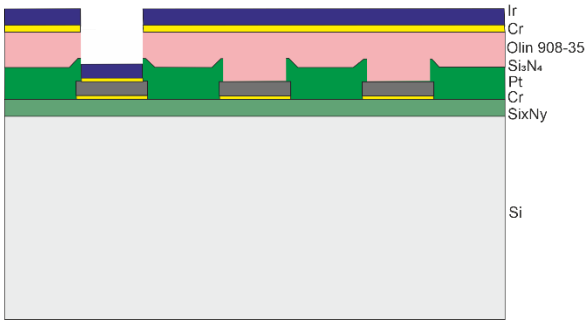

- Deposit an adhesive layer Cr by sputtering
  (Alternatively, Ti can be used)
- Deposit metal, Ir by sputtering

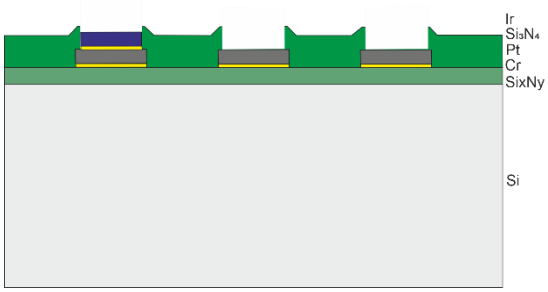

- Strip off the photoresist

End of the lift-off process (2)

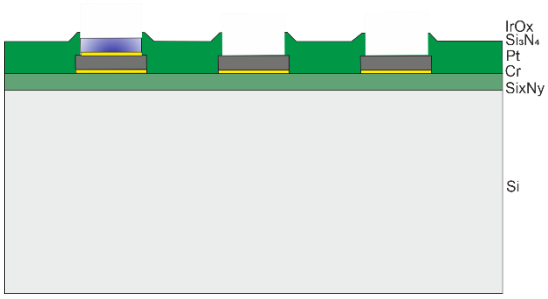

To functionalize RE: Ir to IrOx (Reference electrode)

- Perform cyclic Voltammetry by cycling potential of Ir between hydrogen and oxygen evolution extremes (+0.95V to -0.75) using external Pt strip as CE and Ag/Agcl as RE, leading to the formation of Oxide (IrOx) in a solution containing 0.1M Phosphate buffered Solution (PBS)[21], [22]

End of the formation of IrOx (Reference electrode (RE))

To functionalize working electrode (WE) with enzyme active site

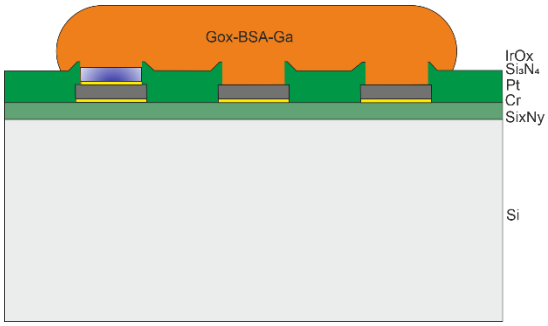

- Drop cast the aqueous solution of 100nL of 3wt% GOx and 3wt% BSA
- Drop cast the aqueous solution of 2wt% glutaraldehyde (crosslinker) [21], [22]
- Dry for 45mins

Figure 36: Schematic representation of cross-section of the design from [21], [22]

APPENDIX B

Process flow for the fabrication of the future device with Au NPs is as follows:

- Prepare a Si substrate or use SOI wafer

- Grow SixNy using LPCVD (thickness is not critical here)

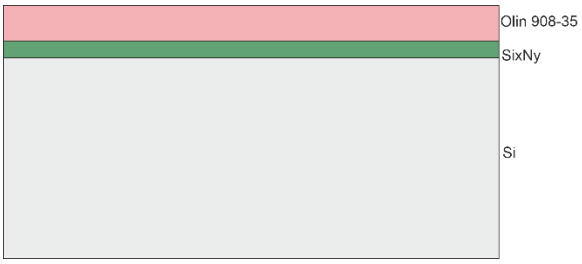

Beginning of lift-off process (1) to deposit Au electrodes

- Spin-coat a lift-off photoresist (Olin 908-35)
- Soft bake

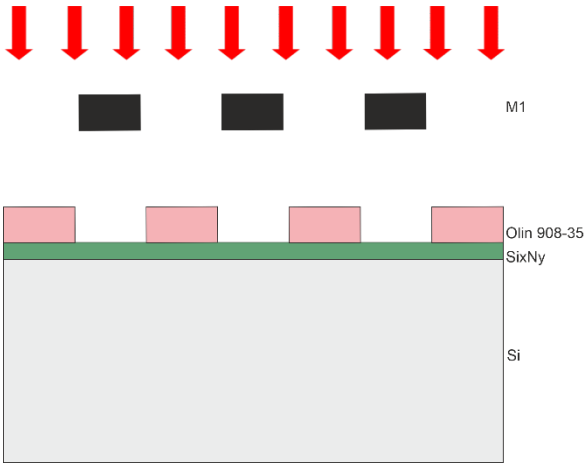

- Expose with the Mask (M1) to pattern trenches, to deposit electrode metal (Au)

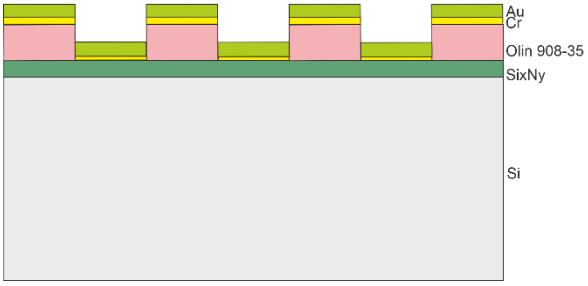

- Deposit an adhesive layer Cr by sputtering
  (Alternatively, Ti can be used)
- Deposit metal, Au by sputtering

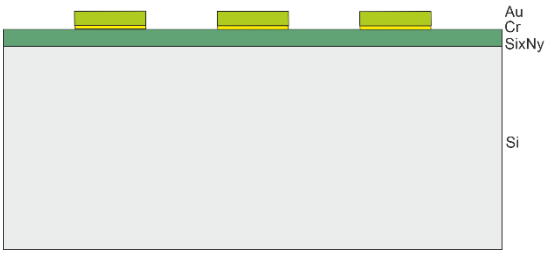

- Strip off the photoresist (Olin 908-35)

End of lift-off process (1)

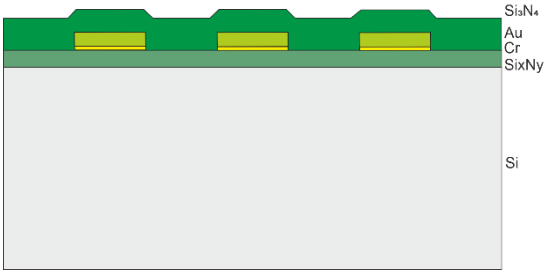

- Deposit a layer of Si_3N_4 using PECVD

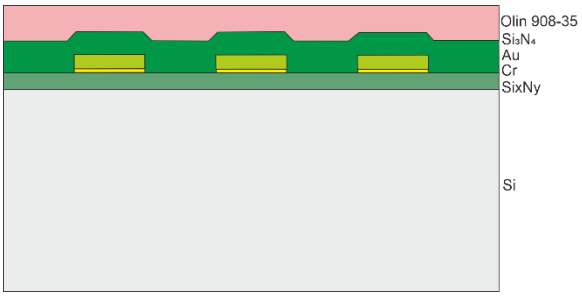

To make openings to the buried electrode under Si_3N_4

- Spin-coat and soft bake photoresist (Olin 908-35)

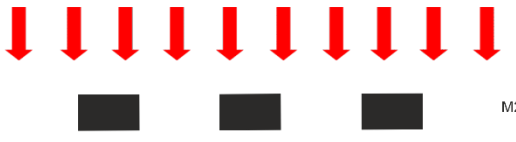

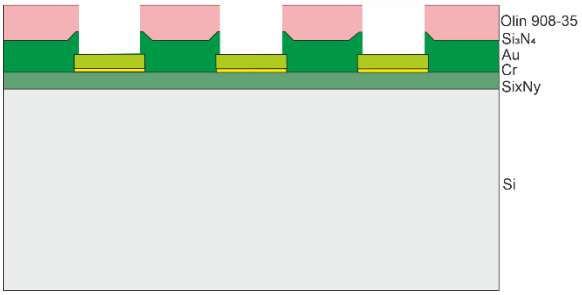

- With the help of IBL or plasma etching
  and mask (M2)
- Pattern the trenches in the photoresist layer and further beyond to the Si_3N_4 layer until it reaches the buried Au metal.

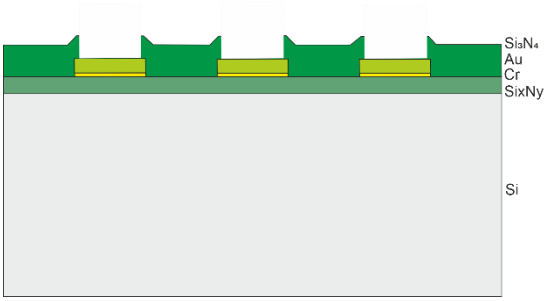

- Strip off the photoresist

End of the formation of the counter electrode (CE)

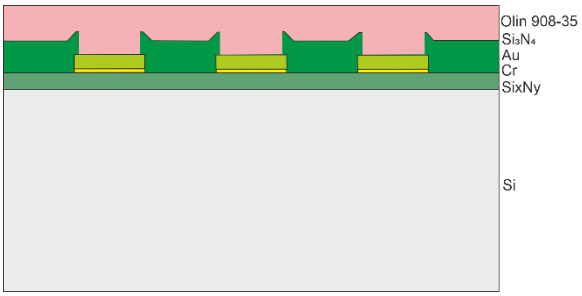

Beginning of the lift-off process (2) to deposit Ir

- Spin-coat and soft bake lift-off photoresist (Olin 908-35)

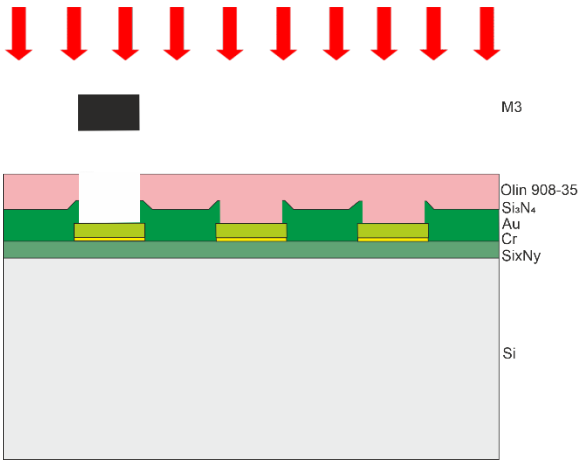

- Expose with the mask (M3)
- Pattern the photoresist to form trench at the target site to deposit Ir

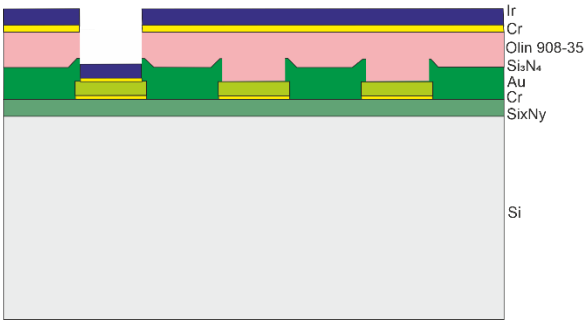

- Deposit an adhesive layer Cr by sputtering
  (Alternatively, Ti can be used)
- Deposit metal, Ir by sputtering

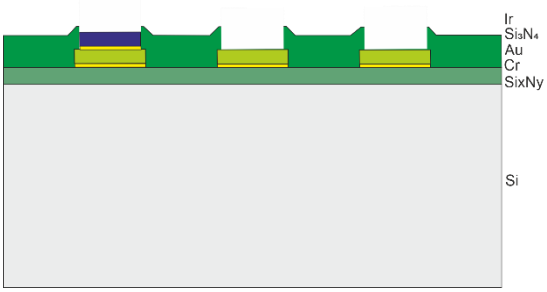

- Strip off the photoresist

End of the lift-off process (2)

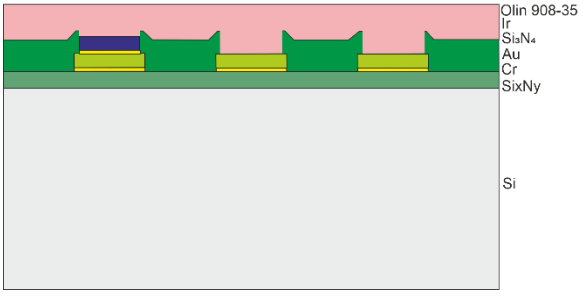

To functionalize working electrode

- Deposit a photoresist by spin-coating

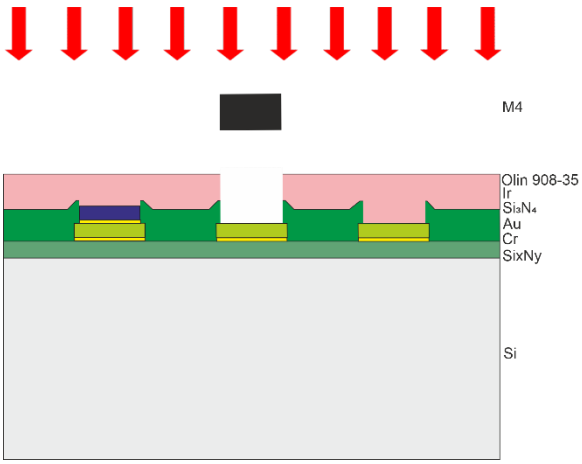

- Pattern trench using mask (M4)

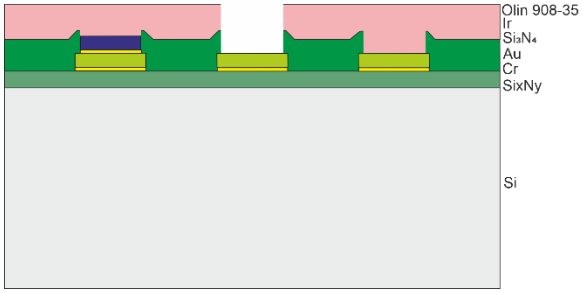

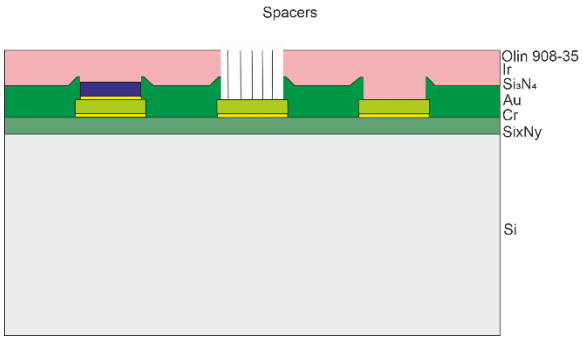

1. *Spacer bridge formation:*

- Place the device in the 2.5mM solution of 1,4-BDMT in dichloromethane overnight (Avoid photooxidation) and wash with dry ethanol. Spacers are self-assembled[33], [35]

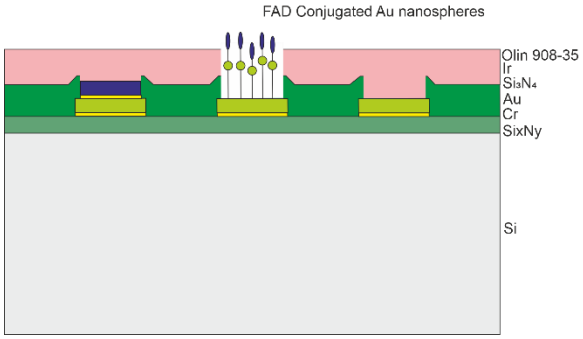

2. *Wiring with ligand conjugated (blue) Au nanospheres (Light green):*

- Self-assembled overnight (Having ready, FAD conjugated Au nanospheres)

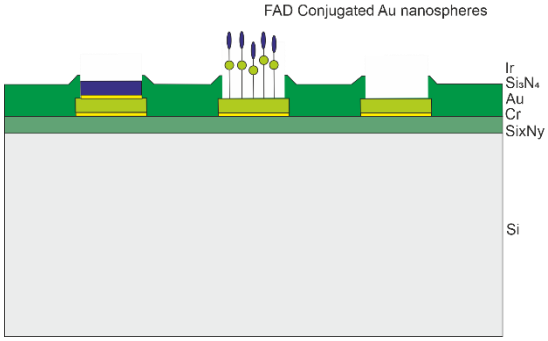

- Strip off the photoresist

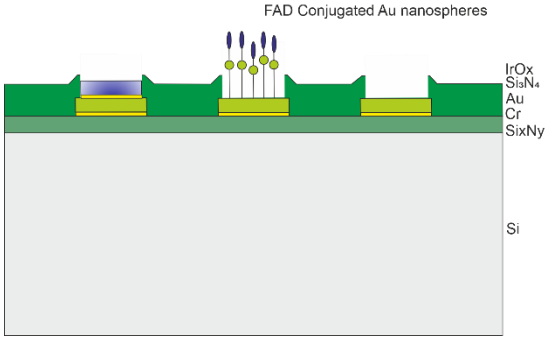

<u>To functionalize RE: Ir to IrOx (Reference electrode)</u>

- Perform cyclic Voltammetry by cycling potential of Ir between hydrogen and oxygen evolution extremes (+0.95V to -0.75) using external Pt strip as CE and Ag/Agcl as RE, leading to the formation of Oxide (IrOx) in a solution containing 0.1M Phosphate buffered Solution (PBS)[21], [22]

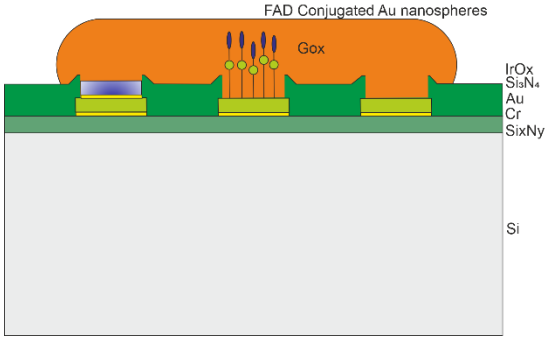

End of the formation of IrOx (Reference electrode (RE))

3. Formation of enzyme active site

- Shake the device in 4mg mL^{-1} apo-GOx in 0.1M phosphate buffer, at pH 7.0 for 4hr at 25°C and 12hr at 4°C
- Rinse by shaking it for 1hr in 0.1M PBS, at pH 7.0 and 0°C [33], [35]

End of functionalization of working electrode with enzyme active site

Figure 37: Schematic representation of cross-section of the advanced design with Au NPs

APPENDIX C

Core spectral analysis of entire sensing area for the three samples is as follows:

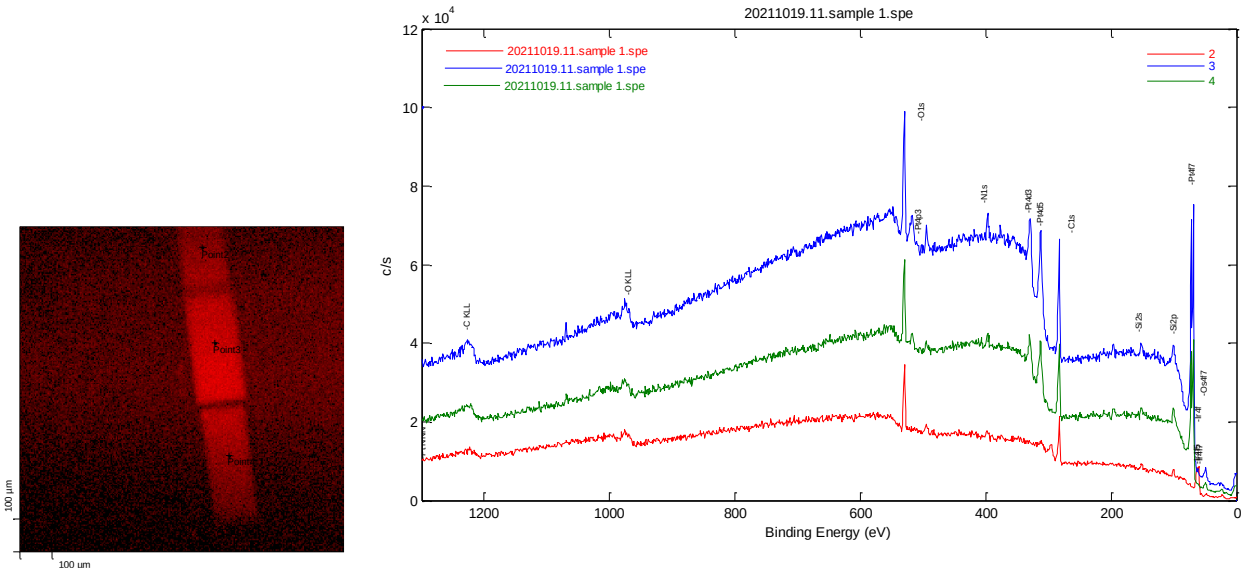

Figure 38: Core spectral analysis of the sensing area for the sample 1

Core spectral analysis was done on sample 1 from binding energies (BE) from -5eV to 1345 eV. It indicated the elements nitride, hydroxides, silicon, platinum and Irridium.

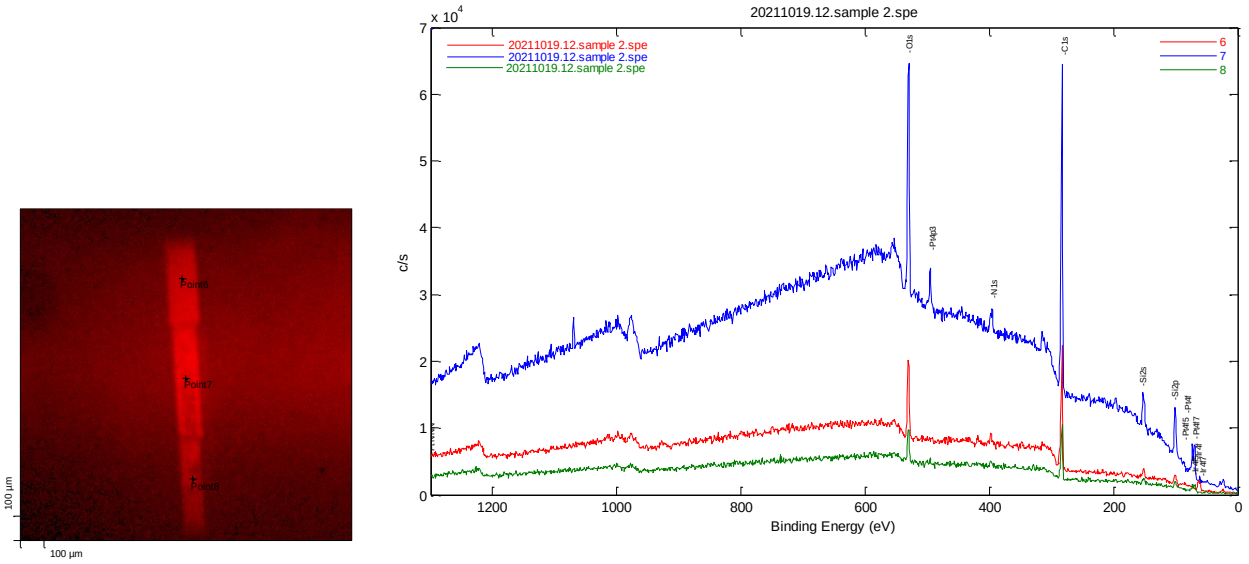

Figure 39: Core spectral analysis of the sensing area for the sample 2

Core spectral analysis was done on sample 2 from binding energies (BE) from -5eV to 1345 eV. It indicated the elements nitride, hydroxides, silicon, platinum and Irridium.

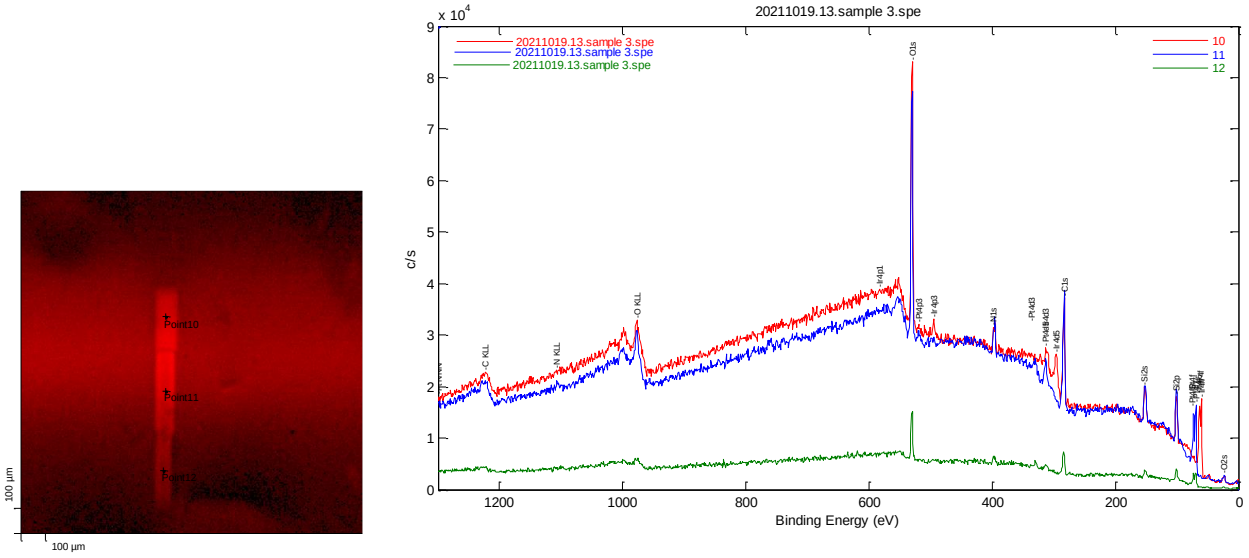

Figure 40: Core spectral analysis of the sensing area for the sample 3

Core spectral analysis was done on sample 3 from binding energies (BE) from -5eV to 1345 eV. It indicated the elements nitride, hydroxides, silicon, platinum and Irridium.

REFERENCE

[1] Y. Saisho, “A focus on beta cell mass could help prevent type 2 diabetes,” *Research Outreach*, no. 119, 2020, doi: 10.32907/ro-119-5053.

[2] M. Heylin, “Facts & Figures,” *Chemical and Engineering*, vol. 57, no. 24. p. 5, 1979. doi: 10.1021/cen-v057n024.p005.

[3] P. Saeedi *et al.*, “Global and regional diabetes prevalence estimates for 2019 and projections for 2030 and 2045: Results from the International Diabetes Federation Diabetes Atlas, 9th edition,” *Diabetes Res Clin Pract*, vol. 157, p. 107843, 2019, doi: 10.1016/j.diabres.2019.107843.

[4] A. Klink, “Diabetes Care in The Netherlands: Improving Health and Wealth,” 2011.

[5] P. Mathew and D. Thoppil, “Hypoglycemia,” *StatPearls*, Jul. 2022.

[6] M. B. M. Mouri, “Hyperglycemia - StatPearls - NCBI Bookshelf,” *StatPearls Publications*, 2021. https://www.ncbi.nlm.nih.gov/books/NBK430900/ (accessed Sep. 21, 2022).

[7] D. Fitzpatrick, *Implantable electronic medical devices*. 2014. doi: 10.1016/c2012-0-07670-3.

[8] N. Ramchandani and R. A. Heptulla, “New technologies for diabetes: a review of the present and the future,” *Int J Pediatr Endocrinol*, no. 1, pp. 1–10, 2012, doi: 10.1186/1687-9856-2012-28.

[9] K. J. Cash and H. A. Clark, “Nanosensors and nanomaterials for monitoring glucose in diabetes,” *Trends Mol Med*, vol. 16, no. 12, pp. 584–593, 2010, doi: 10.1016/j.molmed.2010.08.002.

[10] D. C. Klonoff, D. Ahn, and A. Drincic, “Continuous glucose monitoring: A review of the technology and clinical use,” *Diabetes Res Clin Pract*, vol. 133, pp. 178–192, 2017, doi: 10.1016/j.diabres.2017.08.005.

[11] H. Lee, Y. J. Hong, S. Baik, T. Hyeon, and D. H. Kim, “Enzyme-Based Glucose Sensor: From Invasive to Wearable Device,” *Adv Healthc Mater*, vol. 7, no. 8, pp. 1–14, 2018, doi: 10.1002/adhm.201701150.

[12] G. Piechotta, J. Albers, and R. Hintsche, “Novel micromachined silicon sensor for continuous glucose monitoring,” *Biosens Bioelectron*, vol. 21, no. 5, pp. 802–808, 2005, doi: 10.1016/j.bios.2005.02.008.

[13] A. Rabti, W. Argoubi, and N. Raouafi, “Enzymatic sensing of glucose in artificial saliva using a flat electrode consisting of a nanocomposite prepared from reduced graphene oxide, chitosan, nafion and glucose oxidase,” *Microchimica Acta*, vol. 183, no. 3, pp. 1227–1233, 2016, doi: 10.1007/s00604-016-1753-3.

[14] I. Lee, N. Loew, W. Tsugawa, K. Ikebukuro, and K. Sode, “Development of a third-generation glucose sensor based on the open circuit potential for continuous glucose monitoring,” *Biosens Bioelectron*, vol. 124–125, no. September 2018, pp. 216–223, 2019, doi: 10.1016/j.bios.2018.09.099.

[15] X. Zong and R. Zhu, “ZnO nanorod-based FET biosensor for continuous glucose monitoring,” *Sens Actuators B Chem*, vol. 255, pp. 2448–2453, 2018, doi: 10.1016/j.snb.2017.09.037.

[16] X. Strakosas *et al.*, “A non-enzymatic glucose sensor enabled by bioelectronic pH control,” *Sci Rep*, vol. 9, no. 1, pp. 1–7, 2019, doi: 10.1038/s41598-019-46302-9.

[17] W. Wu, N. Mitra, E. C. Y. Yan, and S. Zhou, “Multifunctional hybrid nanogel for integration of optical glucose sensing and self-regulated insulin release at physiological pH,” *ACS Nano*, vol. 4, no. 8, pp. 4831–4839, 2010, doi: 10.1021/nn1008319.

[18] W. C. Lee *et al.*, “Comparison of enzymatic and non-enzymatic glucose sensors based on hierarchical Au-Ni alloy with conductive polymer,” *Biosens Bioelectron*, vol. 130, no. January, pp. 48–54, 2019, doi: 10.1016/j.bios.2019.01.028.

[19] S. Malhotra, Y. Tang, and P. K. Varshney, “Amperometric enzyme-free glucose sensor based on electrodeposition of Au particles on polyaniline film modified Pt electrode,” *Acta Chim Slov*, vol. 65, no. 3, pp. 1–10, 2018, doi: 10.17344/acsi.2018.4386.

[20] “U-Needle - Microneedle Artificial Pancreas Project.” https://www.uneedle.com/press/microneedle-artificial-pancreas-project (accessed Sep. 21, 2022).

[21] F. Ribet, G. Stemme, and N. Roxhed, “Real-time intradermal continuous glucose monitoring using a minimally invasive microneedle-based system,” *Biomed Microdevices*, vol. 20, no. 4, 2018, doi: 10.1007/s10544-018-0349-6.

[22] F. Ribet, G. Stemme, and N. Roxhed, “Ultra-miniaturization of a planar amperometric sensor targeting continuous intradermal glucose monitoring,” *Biosens Bioelectron*, vol. 90, no. July 2016, pp. 577–583, 2017, doi: 10.1016/j.bios.2016.10.007.

[23] T. C. Dunn, R. C. Eastman, and J. A. Tamada, “Rates of Glucose Change Measured by Blood Glucose Meter and the GlucoWatch Biographer During Day, Night, and Around Mealtimes,” *Diabetes Care*, vol. 27, no. 9, pp. 2161–2165, Sep. 2004, doi: 10.2337/DIACARE.27.9.2161.

[24] “Freestyle Libre 3 Sensor.” https://www.freestyle.abbott/us-en/products/freestyle-libre-3.html (accessed Sep. 21, 2022).

[25] S. Alva *et al.*, “Accuracy of a 14-Day Factory-Calibrated Continuous Glucose Monitoring System With Advanced Algorithm in Pediatric and Adult Population With Diabetes,” *J Diabetes Sci Technol*, vol. 16, no. 1, pp. 70–77, Sep. 2022, doi: 10.1177/1932296820958754.

[26] K. Schlueter, J. Johnson, C. Warner, and W. Miller, “Glucose Analytical Comparability Evaluation of the YSI 2300 STAT Plus™ and YSI 2900D Biochemistry Analyzers Life Sciences Data for Life. TM,” pp. 1–6, 2017.

[27] M. A. Alam, “nanoHUB.org - Courses: nanoHUB-U: Principles of Electronic Nanobiosensors,” *https://nanohub.org/courses/PEN/01a/outline/week2settingtime/l26settingtime-beatingthelimits-dropletevaporation*, 2013. https://nanohub.org/courses/pen (accessed Sep. 22, 2022).

[28] F. G. Banica, *Chemical Sensors and Biosensors Fundamentals and Applications*. 2012.

[29] J. X. J. Zhang and K. Hoshino, *Electrical transducers: Electrochemical sensors and semiconductor molecular sensors*. 2019. doi: 10.1016/b978-0-12-814862-4.00004-1.

[30] G. F. Khan, “TTF-TCNQ Complex Based Printed Biosensor for Long-Term Operation,” *Electroanalysis*, vol. 9, no. 4, pp. 325–329, 1997, doi: 10.1002/elan.1140090413.

[31] F. Palmisano, P. G. Zambonin, D. Centonze, and M. Quinto, “A disposable, reagentless, third-generation glucose biosensor based on overoxidized poly(pyrrole)/tetrathiafulvalene -Tetracyanoquinodimethane composite,” *Anal Chem*, vol. 74, no. 23, pp. 5913–5918, 2002, doi: 10.1021/ac0258608.

[32] R. Pauliukaite, A. Malinauskas, G. Zhylyak, and U. E. Spichiger-Keller, “Conductive organic complex salt TTF-TCNQ as a mediator for biosensors. An overview,” *Electroanalysis*, vol. 19, no. 24, pp. 2491–2498, 2007, doi: 10.1002/elan.200704035.

[33] I. Willner, B. Willner, and R. Tel-Vered, “Electroanalytical applications of metallic nanoparticles and supramolecular nanostructures,” *Electroanalysis*, vol. 23, no. 1, pp. 13–28, 2011, doi: 10.1002/elan.201000506.

[34] B. Willner, E. Katz, and I. Willner, “Electrical contacting of redox proteins by nanotechnological means,” *Curr Opin Biotechnol*, vol. 17, no. 6, pp. 589–596, 2006, doi: 10.1016/j.copbio.2006.10.008.

[35] Y. Xiao, F. Patolsky, E. Katz, J. F. Hainfeld, and I. Willner, “Plugging into enzymes: Nanowiring of redox enzymes by a gold nanoparticle,” *Science (1979)*, vol. 299, no. 5614, pp. 1877–1881, 2003, doi: 10.1126/science.1080664.

[36] J. Liu, A. Chou, W. Rahmat, M. N. Paddon-Row, and J. J. Gooding, “Achieving direct electrical connection to glucose oxidase using aligned single walled carbon nanotube arrays,” *Electroanalysis*, vol. 17, no. 1, pp. 38–46, 2005, doi: 10.1002/elan.200403116.

[37] X. Kang *et al.*, *Controlled activation of iridium film for AIROF microelectrodes*, vol. 190, no. 2013. Elsevier B.V., 2014. doi: 10.1016/j.snb.2013.08.085.

[38] A. Kumar and S. Bankoti, “Synergistic study on electrochemically deposited thin film with a spectrum from micro to nano range structures,” 2009. [Online]. Available: https://www.researchgate.net/publication/37394553

[39] Federico. Ribet, Niclas. Roxhed, G. Stemme, Boris. Stoeber, and KTH Skolan för elektroteknik och datavetenskap (EECS), *Integrated microsystems for continuous glucose monitoring, interstitial fluid sampling and digital microfluidics*.